

A Catalog of Extended Clusters and Ultra-Compact Dwarf Galaxies

An Analysis of their Parameters in Early- and Late-Type Galaxies

R.C. Brüns¹ and P. Kroupa¹

Argelander-Institut für Astronomie, Universität Bonn, Auf dem Hügel 71, D-53121 Bonn, Germany
e-mail: rcbruens@astro.uni-bonn.de, pavel@astro.uni-bonn.de

Received 28 May 2012; accepted 14 September 2012

ABSTRACT

Context. In the last decade, very extended old stellar clusters with masses in the range from a few 10^4 to $10^8 M_{\odot}$ and effective radii larger than 10 pc have been found in various types of galaxies in different environments. Objects with masses comparable to normal globular clusters (GCs) are called extended clusters (ECs), while objects with masses in the dwarf galaxy regime are called ultra-compact dwarf galaxies (UCDs).

Aims. The paper analyses the observational parameters total luminosity, M_V , effective radius, r_{eff} , and projected distance to the host galaxy, R_{proj} , of all known ECs and UCDs and the dependence of these parameters on the type and the total luminosity of their host galaxy.

Methods. We searched the available literature to compile a catalog of star clusters with effective radii larger than 10 pc. As there is no clear distinction between ECs and UCDs, both types of objects will be called extended stellar objects – abbreviated “EOs” – in this paper.

Results. In total, we found 813 EOs of which 171 are associated with late-type galaxies and 642 EOs associated with early-type galaxies. EOs cover a luminosity range from about $M_V = -4$ to -14 mag. However, the vast majority of EOs brighter than $M_V = -10$ mag are associated with giant elliptical galaxies. At each magnitude extended objects are found with effective radii between 10 pc and an upper size limit, which shows a clear trend: the more luminous the object the larger is the upper size limit. For EOs associated with early- and late-type galaxies, the EO luminosity functions peak at -6.40 mag and -6.47 , respectively, which is about one magnitude fainter than the peak of the GC luminosity function. EOs and GCs form a coherent structure in the r_{eff} vs. M_V parameter space, while there is a clear gap between EOs and early type dwarf galaxies. However, there is a small potential overlap at the high-mass end, where the most extended EOs are close to the parameters of some compact elliptical galaxies. We compare the EO sample with the numerical models of a previous paper and conclude that the parameters of the EO sample as a whole can be very well explained by a star cluster origin, where EOs are the results of merged star clusters of cluster complexes (CCs).

Key words. Catalogs, Galaxies: star clusters: general, Galaxies: star clusters: individual: ECs and UCDs

1. Introduction

Globular clusters (GCs) are typically very old stellar objects with masses between $10^4 M_{\odot}$ and $10^6 M_{\odot}$ (corresponding roughly to total luminosities between $M_V = -5$ to $M_V = -10$ mag), having in general compact sizes with half-light radii of a few parsecs. This morphology makes them easily observable also in external galaxies with modern telescopes (see Brodie & Strader, 2006, and references therein).

The Milky Way has a rich GC system containing 157 GCs (Harris, 1996, 2010 edition). Most of them are compact with sizes of a few parsec. Only 13 GCs (or 8%) have an effective radius larger than 10 pc. Most of these extended clusters (ECs) are fainter than $M_V = -7$ mag, only NGC2419, having a half-light radius of about 20 pc, has a high luminosity of about $M_V = -9.4$ mag. Two of the 13 ECs, Arp2 and Terzan8, were classified as Milky Way clusters in Harris (1996, 2010 edition), but the proximity to the Sagittarius dwarf spheroidal galaxy suggests that they are related to this Milky Way satellite (Salinas et al., 2012). Further ECs in the vicinity of the Milky Way have been found in the LMC and the Fornax dwarf galaxy (Mackey & Gilmore, 2004; van den Bergh & Mackey, 2004; McLaughlin & van der Marel, 2005).

Comparable objects have also been detected around other galaxies. Huxor et al. (2005) found three ECs around M31, which have very large radii above 30 pc. These clusters were detected by chance as the automatic detection algorithms of the MegaCam Survey discarded such extended objects as likely background contaminations. Further observations increased the number of ECs in M31 to 13 (Huxor et al., 2008). However, Huxor et al. (2011a) showed that the previous estimates of the effective radii were considerably too large. The new size estimates are well below 30 pc.

In addition to ECs located in galactic halos, Larsen & Brodie (2000) and Brodie & Larsen (2002) have discovered a population of ECs co-rotating with the disk of the lenticular galaxy NGC 1023. These so-called faint fuzzies have similar structural parameters as halo ECs.

Chandar et al. (2004) observed a part of the disks of the nearby spiral galaxies M81, M83, NGC6946, M101, and M51 using HST and found ECs with effective radii larger than 10 pc in four of them. In recent years, hundreds of ECs have been detected in all types of galaxies ranging from dwarfs to giant elliptical galaxies.

Hilker et al. (1999) and Drinkwater et al. (2000) discovered in the Fornax Cluster compact objects with luminosities above

Table 1. Catalog of the 813 EOs presented in this paper.

| | name | r_{eff} (pc) | M_V (mag) | R_{proj} (kpc) | Ref. |
|-----|------------------|--------------------------|----------------|----------------------------|------|
| 1 | MilkyWayEO-01 | 21.4 | -9.42 | 89.9 | 1 |
| 2 | MilkyWayEO-02 | 10.7 | -6.98 | 16.3 | 1 |
| 3 | MilkyWayEO-03 | 13.2 | -6.76 | 17.8 | 1 |
| ... | | | | | |
| 811 | ESO325-G004EO-13 | 60.8 | -11.53 | 24.4 | 51 |
| 812 | ESO325-G004EO-14 | 67.1 | -11.46 | 31.6 | 51 |
| 813 | ESO325-G004EO-15 | 44.1 | -11.34 | 54.5 | 51 |

Notes. This table is available in its entirety in a machine-readable form at the CDS. A portion is shown here for guidance regarding its form and content. The columns denote 1. running number, 2. designation of EO in this paper, 3. effective radius of the EO, 4. absolute V-band luminosity of the EO, 5. projected distance to the host galaxy (for the Milky Way the galacto-centric distance is used), 6. references for the data: (1) Harris (1996), (2) Salinas et al. (2012), (3) van den Bergh & Mackey (2004), (4) Hwang et al. (2011), (5) Huxor et al. (2008), (6) Huxor et al. (2011a), (7) Peacock et al. (2009), (8) Stokutè et al. (2008), (9) Cockcroft et al. (2011), (10) Georgiev et al. (2009), (11) Taylor et al. (2010), (12) Gomez et al. (2006), (13) McLaughlin et al. (2008), (14) Mouhcine et al. (2010), (15) Chattopadhyay et al. (2009), (16) Nantais et al. (2011), (17) Strader et al. (2012), (18) Sharina et al. (2005), (19) van den Bergh (2006), (20) Da Costa et al. (2009), (21) Chandar et al. (2004), (22) Hwang & Lee (2008), (23) Hau et al. (2009), (24) Larsen et al. (2001), (25) Harris et al. (2009), (26) Larsen & Brodie (2000), (27) Norris & Kannappan (2011), (28) Chies-Santos et al. (2011), (29) Hasegan et al. (2005), (30) Chilingarian & Mamon (2008), (31) Evstigneeva et al. (2008), (32) Brodie et al. (2011), (33) Evstigneeva et al. (2007), (34) Chies-Santos et al. (2007), (35) Mieske et al. (2008), (36) Hilker et al. (2007), (37) Richtler et al. (2005), (38) Chilingarian et al. (2011), (39) DeGraaf et al. (2007), (40) Goudfrooij (2012), (41) Blom et al. (2012), (42) Chies-Santos et al. (2006), (43) Cantiello et al. (2009), (44) Da Rocha et al. (2011), (45) Mieske et al. (2007), (46) Misgeld et al. (2011), (47) Penny et al. (2012), (48) Chiboucas et al. (2011), (49) Madrid et al. (2010), (50) Madrid (2011), (51) Blakeslee & Barber (2008)

the brightest known GCs and which were not resolved by ground-based observations. These objects have masses between a few $10^6 M_{\odot}$ and $10^8 M_{\odot}$ and effective radii between $r_{\text{eff}} = 10$ and 100 pc. Phillipps et al. (2001) interpreted these objects as a new type of galaxy and reflected this notion in the name “ultra-compact dwarf galaxy” (UCD). Next to the Fornax Cluster, many UCDs have been found also in other clusters like the Virgo Cluster (Hasegan et al., 2005; Evstigneeva et al., 2007), the Centaurus Cluster (Mieske et al., 2007), the Coma Cluster (Madrid et al., 2010), and the Hydra Cluster (Misgeld et al., 2011). While most known UCDs belong to elliptical galaxies in cluster environments, they have also been observed in rather isolated objects like the Sombrero galaxy M104 (Hau et al., 2009) or the group elliptical NGC3923 (Norris & Kannappan, 2011).

A number of different origins of UCDs were brought up next to the original proposal of UCDs being just a new type of galaxy (Phillipps et al., 2001). Bekki et al. (2001, 2003) suggested that UCDs are the remnants of dwarf galaxies which lost their dark matter halo and all stars except for their nucleus. Next to the interpretation as a galaxy, UCDs were also considered as high-mass versions of normal GCs (Mieske et al., 2002), or as merged massive complexes of star clusters (Kroupa, 1998; Fellhauer & Kroupa, 2002a; Bekki et al., 2004). Forbes et al. (2008) and Mieske et al. (2008) analyzed the parameters of UCDs and concluded that UCDs are more likely bright ex-

tended clusters than naked cores of stripped dwarf galaxies. The marginally enhanced mass-to-light ratios of UCDs can be explained by slightly modified initial stellar mass functions (Mieske & Kroupa, 2008; Dabringhausen et al., 2009).

High-resolution HST imaging of gas-rich galaxies experiencing major interactions has resolved very intense star formation bursts. Bastian et al. (2006a) observed star cluster complexes (CCs), i.e. clusters of young massive star clusters, in the Antennae with masses of the order $\approx 10^6 M_{\odot}$ and diameters of the order 100 to 200 pc. Whitmore et al. (2005) found that the cluster to cluster velocity dispersion in some CCs in the Antennae, aka the knots, is small enough to keep them gravitationally bound. Pellerin et al. (2010) detected young massive CCs with masses between $10^6 M_{\odot}$ and $10^{7.5} M_{\odot}$ and diameters between 600 pc and 1200 pc in the collisional ring galaxy NGC 922. One of the most extended CCs has been observed by Tran et al. (2003) in the tail of the “Tadpole galaxy” UGC 10214. This CC, which has a mass of the order $10^6 M_{\odot}$, has an effective radius of 160 pc and a diameter of about 1500 pc. In a previous paper, we proposed a common origin of ECs and UCDs based on the merged star cluster scenario (Brüns et al., 2011). We performed a parametric study that systematically scanned a suitable parameter space of CCs and performed numerical simulations to study their further evolution. We concluded that the observed ECs and UCDs can be well explained as evolved star CCs.

In recent years, the number of observed ECs and UCDs has rapidly increased for all types of galaxies in various environments. As there is no clear distinction between ECs and UCDs, both types of objects will be called extended stellar objects – abbreviated “EOs” – in this paper. The high number of EOs known today, allows for the first time for a detailed analysis of the properties of EOs to disclose commonalities and distinctions of objects from early- and late-type galaxies.

The paper is structured as follows: in Section 2 we compile a catalog of ECs and UCDs on the basis of the available publications containing structural parameters of ECs and UCDs. In Section 3 we present the results of the catalog that are discussed in Section 4. Section 5 provides a summary and conclusions.

2. Observational basis

As already indicated in the previous section, GC-like objects with effective radii above 10 pc, which cover a large luminosity range, have been found in various environments from dwarf to giant elliptical galaxies. To allow for an analysis of their parameters, we compiled a catalog of effective radii, absolute V-band luminosities, and projected distances of EOs to their host galaxies as well as the absolute V-band luminosities of these galaxies and their distance to the Milky Way. We distinguish between EOs found in late-type galaxies, i.e. spiral and irregular galaxies, and early-type galaxies, i.e. elliptical, lenticular, and dwarf spheroidal galaxies. In Table 1, available at the CDS, we present the catalog of the 813 EOs used in this study. Table 2 provides an overview on the galaxies, where EOs were detected, the number of EOs per galaxy and the luminosity range of the detected EOs.

2.1. EOs in Late-Type Galaxies

According to the 2010 edition of the GC catalog of Harris (1996) and considering that Arp2 and Terzan8 are associated with the Sagittarius dwarf spheroidal galaxy (Salinas et al., 2012), the Milky Way has 11 EOs. The other two Local Group spiral galaxies M31 and M33 have 20 (Huxor et al., 2008;

Table 2. Catalog of the 65 galaxies containing EOs.

| Galaxy | Type | $M_{V,gal}$ (mag) | D_{gal} (kpc) | $Pi_{X_{HST}}$ (pc) | N_{EO} | $M_{V,EO,min}$ (mag) | $M_{V,EO,max}$ (mag) | N_{GC} | Ref |
|-------------|------|----------------------|--------------------|------------------------|----------|-------------------------|-------------------------|----------|-------------------|
| Milky Way | LT | -20.5 | 0 | | 11 | -4.73 | -9.42 | 142 | 1 |
| SAGdSph | LT | -13.8 | 27 | | 2 | -5.41 | -5.68 | 2 | 2 |
| LMC | LT | -18.34 | 50 | | 4 | -4.37 | -7.25 | 12 | 3 |
| Fornax | ET | -13.3 | 138 | | 1 | -5.32 | -5.32 | 0 | 3 |
| NGC6822 | LT | -16 | 470 | 0.1 | 3 | -6.06 | -7.7 | 3 | 4 |
| M31 | LT | -21.8 | 780 | 0.2 | 20 | -4.4 | -7.68 | 232 | 5;6;7 |
| M33 | LT | -19.4 | 870 | 0.2 | 2 | -5.9 | -6.6 | 4 | 8;9 |
| UGCA86 | LT | -13.55 | 2728 | 0.7 | 1 | -7.58 | -7.58 | 11 | 10 |
| UGC8638 | LT | -13.8 | 3285 | 0.8 | 1 | -6.57 | -6.57 | 2 | 10 |
| NGC247 | LT | -19.4 | 3636 | 0.9 | 2 | -6.59 | -7.42 | 0 | 10 |
| NGC5128 | ET | -21.4 | 3676 | 0.9 | 26 | -5.2 | -11.17 | 194 | 11;12;13;14;15 |
| M81 | LT | -21.2 | 3692 | 0.9 | 44 | -4.53 | -8.59 | 369 | 16 |
| NGC4449 | LT | -18.28 | 3693 | 0.9 | 7 | -5.35 | -7.14 | 99 | 17 |
| IKN | ET | -11.5 | 3680 | 0.9 | 1 | -6.76 | -6.76 | 4 | 10 |
| NGC5237 | LT | -15.7 | 3794 | 0.9 | 1 | -6.85 | -6.85 | 2 | 10 |
| ESO269-58 | LT | -16.3 | 3825 | 0.9 | 2 | -6.62 | -6.86 | 6 | 10 |
| UGC7605 | LT | -13.8 | 4177 | 1 | 1 | -6.44 | -6.44 | 0 | 18;19 |
| ScI-dE1 | ET | -11.1 | 4300 | 1 | 1 | -6.7 | -6.7 | 0 | 20 |
| KK065 | LT | -13.32 | 4510 | 1.1 | 1 | -6.75 | -6.75 | 0 | 18;19 |
| NGC784 | LT | -17.6 | 4560 | 1.1 | 2 | -6.4 | -6.62 | 5 | 10 |
| M83 | LT | -21 | 4659 | 1.1 | 1 | -8.24 | -8.24 | 20 | 21 |
| NGC4605 | LT | -18.5 | 4730 | 1.1 | 2 | -6.34 | -8.26 | 9 | 10 |
| UGC3974 | LT | -15.2 | 4897 | 1.2 | 1 | -8.72 | -8.72 | 4 | 10 |
| UGC3755 | LT | -15 | 5166 | 1.3 | 2 | -6.09 | -7.54 | 30 | 18;19 |
| KK112 | LT | -12.28 | 5220 | 1.3 | 2 | -6.21 | -6.77 | 1 | 18;19 |
| NGC1311 | LT | -16.3 | 5252 | 1.3 | 1 | -7.33 | -7.33 | 5 | 10 |
| UGC4115 | LT | -14.12 | 5508 | 1.3 | 1 | -6 | -6 | 2 | 18;19 |
| M51 | LT | -21.4 | 8031 | 1.9 | 21 | -6.91 | -8.86 | 2203 | 22 |
| M104 | LT | -22.45 | 9000 | 2.2 | 10 | -6.05 | -12.3 | 184 | 23;24 |
| NGC891 | LT | -21.2 | 9700 | 2.4 | 6 | -5.16 | -7.3 | 37 | 25 |
| KK84 | ET | -14.4 | 10069 | 2.4 | 6 | -6.64 | -9.68 | 1 | 18;19 |
| NGC1023 | ET | -21.2 | 11791 | 2.9 | 15 | -6.02 | -7.13 | 14 | 26 |
| NGC4546 | ET | -20.9 | 13060 | 3.2 | 1 | -12.94 | -12.94 | 0 | 27 |
| NGC4660 | ET | -19.69 | 14875 | 3.6 | 1 | -8.34 | -8.34 | 50 | 28 |
| IC3652 | ET | -18.7 | 14960 | 3.6 | 1 | -11.95 | -11.95 | 0 | 29 |
| NGC4278 | ET | -20.78 | 15154 | 3.7 | 1 | -9.93 | -9.93 | 66 | 28 |
| NGC4486B | ET | -17.64 | 15450 | 3.7 | 1 | -11.98 | -11.98 | 0 | 29 |
| M89 | ET | -21.32 | 15574 | 3.8 | 3 | -10.44 | -11.6 | 104 | 28;29 |
| M59 | ET | -21.38 | 15821 | 3.8 | 1 | -13.3 | -13.3 | 0 | 30 |
| M49 | ET | -22.63 | 16052 | 3.9 | 1 | -10.47 | -10.47 | 0 | 29 |
| M86 | ET | -22.21 | 16321 | 4 | 2 | -9.08 | -9.66 | 74 | 28 |
| NGC4476 | ET | -18.97 | 16450 | 4 | 1 | -10.89 | -10.89 | 0 | 29 |
| M87 | ET | -22.54 | 16675 | 4 | 51 | -8.1 | -13.42 | 301 | 28;29;31;32 |
| M85 | ET | -21.98 | 17382 | 4.2 | 4 | -8.5 | -11.46 | 55 | 28;29 |
| M84 | ET | -22.12 | 17422 | 4.2 | 1 | -9.75 | -9.75 | 92 | 28 |
| NGC1380 | ET | -21.3 | 18221 | 4.4 | 13 | -5.14 | -9.45 | 174 | 34 |
| NGC1399 | ET | -21.88 | 18950 | 4.6 | 18 | -10.02 | -13.4 | 18 | 31;33;35;36;37;38 |
| NGC1533 | ET | -20.7 | 19400 | 4.7 | 3 | -7.04 | -7.52 | 136 | 39 |
| NGC3923 | ET | -21.9 | 21280 | 5.2 | 3 | -11.29 | -12.43 | 0 | 27 |
| NGC1316 | ET | -22.91 | 21900 | 5.3 | 45 | -5.65 | -9.26 | 433 | 40 |
| NGC4365 | ET | -22.13 | 23100 | 5.6 | 217 | -4.66 | -11.84 | 2038 | 41 |
| NGC5846 | ET | -22.18 | 26709 | 6.5 | 13 | -6.89 | -9.32 | 41 | 42 |
| NGC3370 | LT | -20 | 27376 | 6.6 | 22 | -5.51 | -7.61 | 255 | 43 |
| NGC1199 | ET | -21.25 | 33100 | 8 | 2 | -11.97 | -12.15 | 8 | 44 |
| NGC4696 | ET | -22.81 | 37582 | 9.1 | 2 | -11.1 | -11.52 | 6 | 45 |
| NGC3311 | ET | -22.2 | 47200 | 11.4 | 19 | -9.29 | -13.35 | 7 | 46 |
| NGC1275 | ET | -22.72 | 71000 | 17.2 | 84 | -9.98 | -13.33 | 0 | 47 |
| IC4041 | ET | -20.74 | 94400 | 22.9 | 4 | -10.77 | -11.31 | 0 | 48 |
| NGC4889 | ET | -23.51 | 94400 | 22.9 | 2 | -11.11 | -11.34 | 2 | 48 |
| IC3998 | ET | -20.43 | 98950 | 24 | 1 | -11.79 | -11.79 | 0 | 48 |
| IC4030 | ET | -19.6 | 98950 | 24 | 2 | -10.7 | -11.41 | 0 | 48 |
| NGC4874 | ET | -23.25 | 98950 | 24 | 36 | -9.85 | -14.03 | 2 | 48;49 |
| NGC1132 | ET | -22.65 | 99500 | 24.1 | 39 | -9.24 | -14.8 | 11 | 50 |
| NGC4908 | ET | -21.82 | 101114 | 24.5 | 3 | -11.08 | -12.47 | 0 | 48 |
| ESO325-G004 | ET | -23.2 | 143000 | 34.7 | 15 | -11.34 | -13.51 | 0 | 51 |

Notes. The columns denote 1. name of the galaxy, 2. type of host galaxy (LT: late-type, ET: early-type), 3. absolute V-band luminosity of the galaxy, 4. distance of the galaxy, 5. size of a HST ACS pixel at the distance of the galaxy, 6. number of EOs, 7. minimum absolute V-band luminosity of the EO, 8. maximum absolute V-band luminosity of the EO, 9. number of GCs in the same publications, 10. references as in Table 1

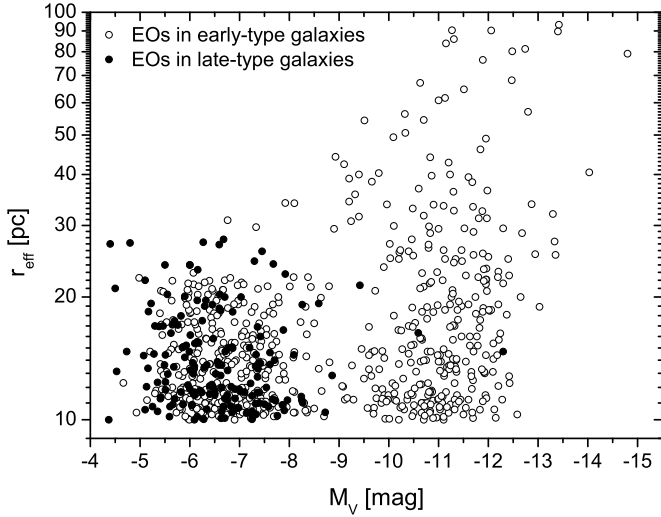


Fig. 1. Effective radii of EOs are plotted against their absolute V-band luminosities. EOs associated with early-type galaxies are plotted as open circles, EOs associated with late-type galaxies are plotted as black circles.

Peacock et al., 2009; Huxor et al., 2011a) and 2 (Stonkutė et al., 2008; Cockcroft et al., 2011) EOs, respectively. EOs were also found in the LMC (van den Bergh & Mackey, 2004), and the dwarf irregular galaxy NGC6822 (Hwang et al., 2011).

Outside the Local Group, EOs were detected in the spiral galaxies M81 (Chandar et al., 2004; Nantais et al., 2011), M83 (Chandar et al., 2004), M51 (Chandar et al., 2004; Hwang & Lee, 2008), NGC891 (Harris et al., 2009), NGC3370 (Cantiello et al., 2009), and in the Sombrero Galaxy M104 (Larsen et al., 2001; Hau et al., 2009). In addition, EOs were found in the dwarf irregular and the Magellanic type dwarf galaxies UGCA86, UGC8638, NGC247, NGC5237, ESO269-58, NGC784, NGC4605, UGC3974, and NGC1311 (Georgiev et al., 2009), UGC7605, KK065, UGC3755, KK112, and UGC4115 (Sharina et al., 2005; van den Bergh, 2006), and NGC4449 (Strader et al., 2012).

In total, the EO catalog contains 171 EOs associated with late-type galaxies.

2.2. EOs in Early-Type Galaxies

EOs were detected in a large number of elliptical galaxies: NGC5128 (Gomez et al., 2006; McLaughlin et al., 2008; Chattopadhyay et al., 2009; Taylor et al., 2010; Mouhcine et al., 2010), NGC4660 (Chies-Santos et al., 2011), IC3652 (Haşegan et al., 2005), NGC4278 (Chies-Santos et al., 2011), NGC4486B (Haşegan et al., 2005), M89 (Haşegan et al., 2005; Chies-Santos et al., 2011), M59 (Chilingarian & Mamon, 2008), M49 (Haşegan et al., 2005), M86 (Chies-Santos et al., 2011), the central galaxy of the Virgo Cluster M87 (Haşegan et al., 2005; Evstigneeva et al., 2008; Brodie et al., 2011; Chies-Santos et al., 2011), M84 (Chies-Santos et al., 2011), the central galaxy of the Fornax Cluster NGC1399 (Richtler et al., 2005; Evstigneeva et al., 2007; Hilker et al., 2007; Evstigneeva et al., 2008; Mieske et al., 2008; Chilingarian et al., 2011), NGC3923 (Norris & Kannappan, 2011), NGC4476 (Haşegan et al., 2005), NGC5846 (Chies-Santos et al., 2006), NGC4696 (Mieske et al., 2007), NGC3311 (Misgeld et al., 2011), IC4041, NGC4889, IC3998, IC4030, IC4041, and NGC4908 (Chiboucas et al., 2011), NGC4874 (Madrid et al., 2010; Chiboucas et al.,

2011), NGC1132 (Madrid, 2011), NGC1275 (Penny et al., 2012), NGC4365 (Blom et al., 2012), NGC1316 (Goudfrooij, 2012), NGC1199 (Da Rocha et al., 2011), and ESA325-G004 (Blakeslee & Barber, 2008).

In five lenticular galaxies, EOs were detected: in NGC1023 (Larsen & Brodie, 2000; Brodie & Larsen, 2002) and NGC1380 (Chies-Santos et al., 2007), 15 and 13 EOs were found, respectively. One EO was discovered in NGC4546 (Norris & Kannappan, 2011), three EOs in NGC1533 (DeGraaf et al., 2007), and four EOs were found in M85 (Haşegan et al., 2005; Chies-Santos et al., 2011).

The EO of the dwarf elliptical Scl-dE1 (Da Costa et al., 2009), the two EOs of the Sagittarius dSph galaxy (Salinas et al., 2012), the EO of the dSph galaxy Fornax (van den Bergh & Mackey, 2004), the 6 EOs of the dSph galaxy KK84 (Sharina et al., 2005; van den Bergh, 2006), and the EO of the dSph galaxy IKN (Georgiev et al., 2009) are contributing to the list of EOs associated with early-type galaxies.

In total, 642 EOs were found in early-type galaxies, 595 thereof are associated with elliptical galaxies. The EO sample of the elliptical galaxies is dominated by the two galaxies NGC4365 and NGC1275, which have 217 and 84 EO candidates, respectively.

3. Results

3.1. Correlations between the Parameters of Extended Objects

Figure 1 shows the effective radii r_{eff} of the 813 EOs of our catalog as a function of their total V-band luminosities M_V . The vast majority of EOs associated with late-type galaxies have magnitudes between $M_V = -4$ to -9 mag. Only three EOs, the Milky Way cluster NGC2419 and two EOs associated with the Sombrero Galaxy M104, have total V-band luminosities brighter than $M_V = -9$ mag. EOs associated with early-type galaxies cover a significantly larger range of V-band luminosities. The majority of objects are found in the magnitude range of about $M_V = -5$ to -13 mag. At $M_V = -8.5$ mag the number of objects is much smaller than for lower and higher luminosities.

At each magnitude EOs are found with effective radii between 10 pc and an upper size limit, which shows a clear trend: the more luminous the object the larger is the upper size limit.

The dependency of the structural parameters effective radius, r_{eff} , and luminosity, M_V , of EOs on the projected distance from their host galaxy, R_{proj} , are displayed in Figure 2. For late-type galaxies there is a slight trend of increasing effective radii and decreasing total luminosities with increasing projected distance (Fig. 2a and c). On the other hand, very faint and very extended objects are extremely hard to detect at very low projected distances due to the high surface brightness of the underlying host galaxy. Consequently, the slight trends might not be significant. In early-type galaxies the most extended objects are found predominantly at large projected distances (Fig. 2b). The most extended EO, VUCD7, with an effective radius of 93.2 pc, was discovered in the central elliptical galaxy M87 of the Virgo Cluster at a projected distance of 82.6 kpc. In early-type galaxies, the low-luminosity objects are comparable to those in late-type galaxies and there are high-luminosity objects that are not present in late-type galaxies. The void at projected distances larger than about 70 kpc and luminosities fainter than -10.5 mag is a result of the limited coverage and sensitivity of most surveys.

Figure 3 shows two histograms of the number of EOs with different total V-magnitudes. The EOs in late-type galaxies have

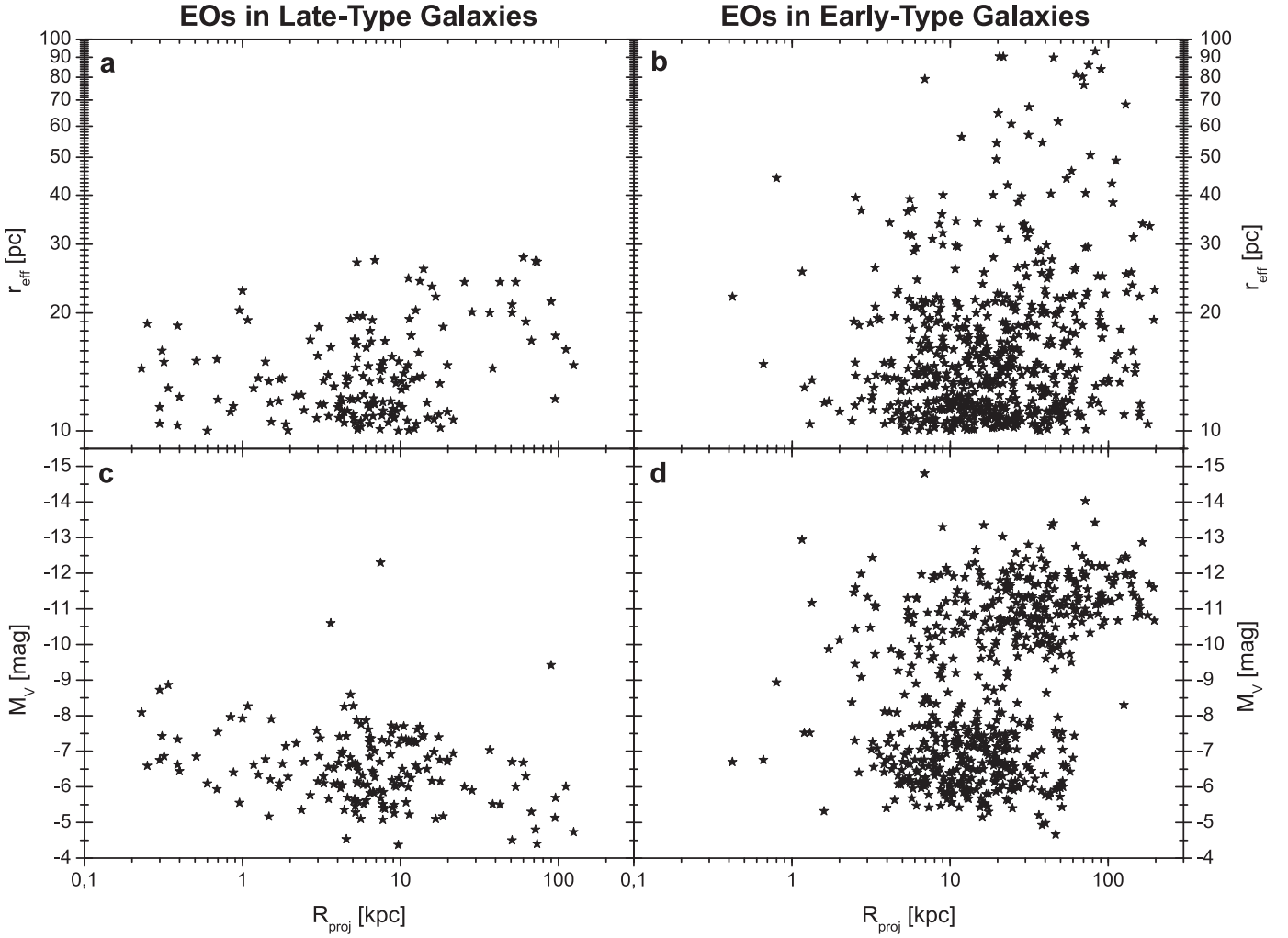


Fig. 2. (a) and (b) Effective radii of EOs are plotted against the projected distances to their host galaxies. (c) and (d) Absolute V-magnitudes of EOs are plotted against the projected distance.

a luminosity distribution which peaks at around $M_V = -6.5$ mag, while the EOs in early-type galaxies show a bimodal distribution which peaks at $M_V = -6.5$ mag and -11.0 mag and has a clear minimum between -8.5 and -9 mag. In Section 4.2.2, it will be shown that the bimodal luminosity distribution is mostly a selection effect due to EO samples covering solely the high luminosity regime.

Figure 4 shows two histograms of the number of EOs with different effective radii. For EOs in both early- and late-type galaxies, the majority of objects has small effective radii. The mean size for EOs in early-type galaxies is 18.1 pc and its median value lies at 14.2 pc. For EOs in early-type galaxies that are fainter than $M_V = -10$ mag, the mean and the median size are 15.2 pc and 13.5 pc, respectively. The sizes of EOs in late-type galaxies are slightly smaller: the mean size is 14.4 pc and its median value is 13.2 pc. For EOs in late-type galaxies, 39.2% have effective radii between 10 and 12 pc. For early-type galaxies, 38.8% and 25.0% are in the interval between 10 and 12 pc for EOs fainter and brighter than $M_V = -10$ mag, respectively.

A histogram of the projected distance of EOs to their host galaxies is presented in Figure 5. EOs in late-type galaxies were predominantly found at small projected distances below 20 kpc. It should be noted, however, that the coverage of the halo beyond projected distances of 20 kpc is extremely poor for most late-type galaxies. EOs in early-type galaxies were found also

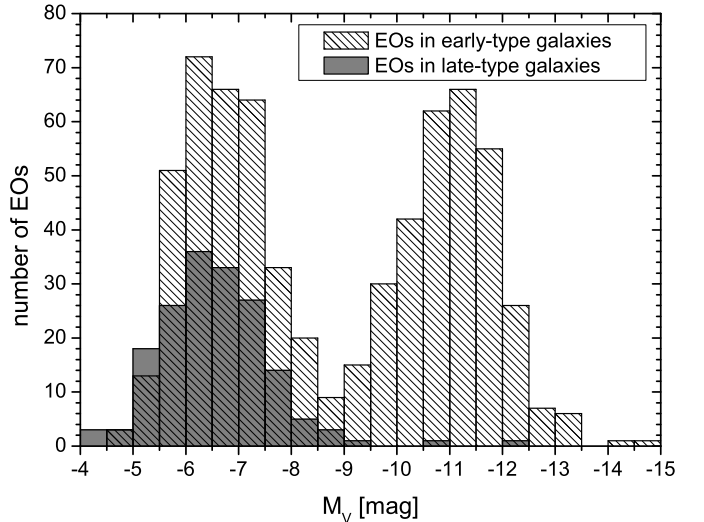


Fig. 3. Histogram of the number of EOs in early-type and late-type galaxies at different total V-band luminosities.

at considerably larger distances. The mean and the median projected distances are 12.9 kpc and 6.4 kpc for EOs in late-type

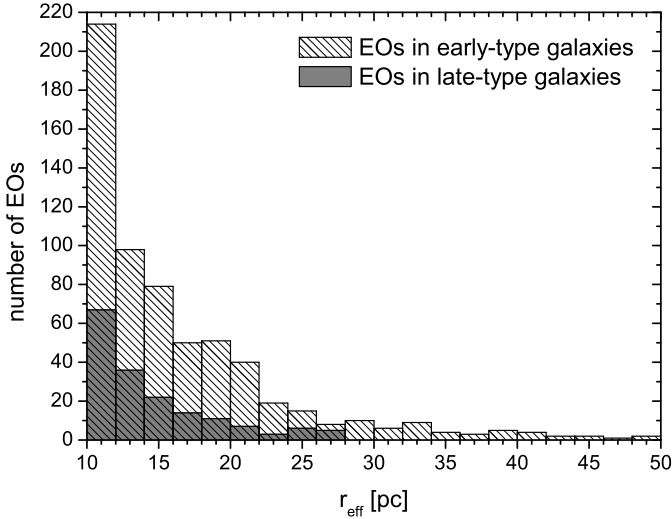


Fig. 4. Histogram of the number of EOs in early-type and late-type galaxies at different effective radii.

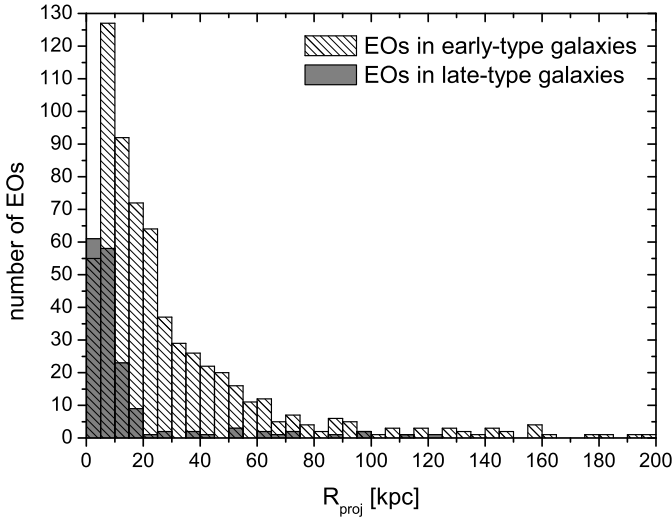


Fig. 5. Histogram of the number of EOs in early-type and late-type galaxies at different projected radii.

galaxies and 28.7 kpc and 17.9 kpc for EOs in early-type galaxies, respectively. Only few EOs have been discovered beyond 100 kpc. All EOs with projected distances larger than 130 kpc are associated with the giant elliptical galaxies in the center of the Virgo Cluster, the Fornax Cluster, the Perseus Cluster, and the Coma Cluster. This result does not necessarily imply that only the central galaxies of clusters have EOs at very large distances, as rather isolated galaxies scarcely have HST observations at such large projected distances (see Sect. 4.3).

3.2. Correlation of EO parameters with those of their host galaxies.

Figure 6 shows the dependence of the parameters projected distance of EOs to their host galaxies, R_{proj} , effective radius, r_{eff} , and absolute V-band magnitude of the EOs, $M_{V,\text{EO}}$, on the total V-band luminosity of the host galaxies, $M_{V,\text{gal}}$.

Figures 6a and b illustrate the dependence of the projected distances of the EOs on the total V-band luminosity of the host galaxies. For EOs in late-type galaxies only three galaxies (the

Local Group galaxies Milky Way, M31, and M33) host EOs at projected distances beyond 20 kpc. In contrast, for early-type galaxies with luminosities between -21 and -24 mag EOs are found far out from the galactic center even beyond 100 kpc. Only very few objects are found at projected distances less than a few kiloparsecs. This lack of EOs at small projected distances is at least partly due to the fact that EOs have a very low contrast on the bright background light from the host galaxy.

Figures 6c and d demonstrate that the upper limit of the effective radii of EOs in late-type and early-type galaxies tends to increase with the total V-band luminosity of the host galaxy. For all galaxies, most EOs have effective radii well below 20 pc.

Figure 6e shows that the total luminosity of EOs in late-type galaxies does not depend on the total luminosity of their host galaxy. For EOs in early-type galaxies (Fig. 6f) there is a trend: the more massive the parent galaxy the higher is the upper limit of the luminosities of its EOs. This trend is partly a size-of-sample effect, as in large EO samples also extreme luminosities can be realized. In Section 4.2.2 we will demonstrate, however, that the number of high-luminosity objects is larger than expected from the EO luminosity function.

Figure 7a plots the projected distances of the EOs versus the distance of their host galaxies from the Galaxy. Early-type galaxies have been studied nearby as well as at large distances up to 143 Mpc, while late-type galaxies were mainly observed in the local universe up to distances of 10 Mpc. Only one spiral (NGC 3370) was searched for EOs at a larger distance of about 27 Mpc.

Figure 7b displays the absolute V-magnitude of the EOs versus the distance of the host galaxy from the Galaxy. The maximum absolute V-magnitude of EOs does not change with the distance of the host galaxy. While EOs brighter than $M_V = -10$ mag were detected at all distances, faint EOs have only been observed in galaxies closer than 30 Mpc.

4. Discussion

4.1. Distribution in the r_{eff} vs. M_V space.

Figure 1 shows the effective radii r_{eff} of the 813 EOs as a function of their total V-band luminosities M_V . At all luminosities, EOs cover a range between 10 pc and an upper limit, which increases with increasing luminosity from about 25 pc at $M_V = -5$ mag to about 100 pc at $M_V = -13$ mag.

This trend of the increasing upper limit of effective radii with total luminosities defines the range where EOs have been found so far. It should not, however, be regarded as a firm upper limit, as very extended objects with a low total luminosity are extremely hard to detect. While the detection limit of EOs depends on numerous parameters like the magnitude and the structure of the fore- and background emission, we will focus on the characteristics of the EOs themselves.

The effective radius is defined as the radius where half of the total luminosity of an object is included. A large effective radius means that the luminosity is spread over a large area leading to low surface brightness. In order to provide a rough estimate of the mean surface brightness, we divide the luminosity within the effective radius by the area of a circle with the size of the effective radius,

$$\overline{\Sigma}_{V,\text{EO}} = \frac{0.5 L_{V,\text{EO}}}{A(r_{\text{eff}})} = \frac{10^{-0.4(M_V - M_{V,\odot})}}{2\pi r_{\text{eff}}^2} \quad (1)$$

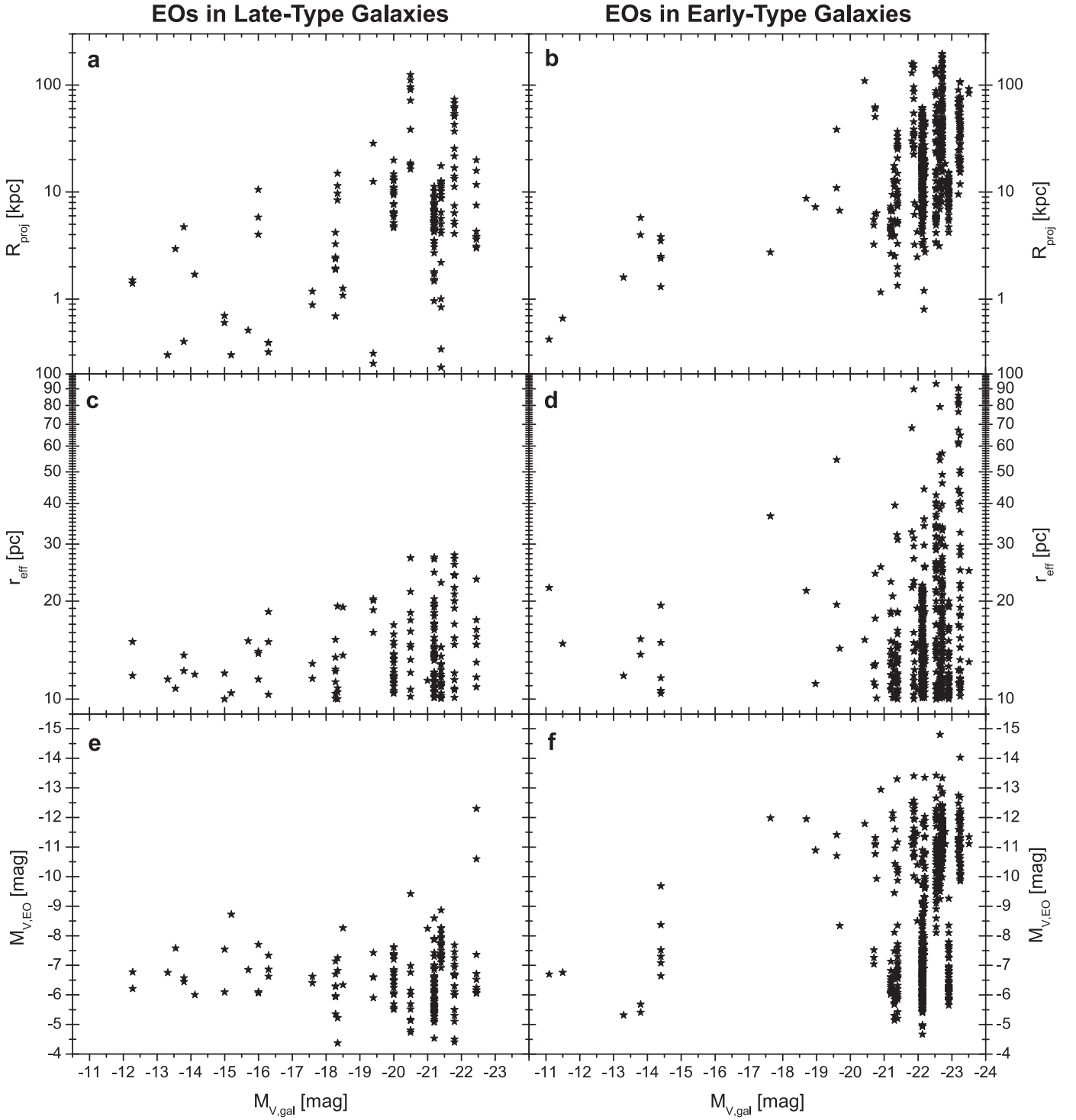


Fig. 6. (a) and (b) Projected distances of EOs are plotted against the total V-band luminosity of their host galaxies. (c) and (d) Effective radii of EOs are plotted against the total V-band luminosity of the host galaxies. (e) and (f) Absolute V-magnitudes of EOs are plotted against the total V-band luminosity of the host galaxies.

where $\overline{\Sigma}_{V,\text{EO}}$ is the mean surface brightness, $L_{V,\text{EO}}$ is the total luminosity of an EO, $M_{V,\odot} = 4.83$ mag is the absolute solar V-band luminosity, and $A(r_{\text{eff}}) = \pi r_{\text{eff}}^2$ is the area within r_{eff} . Figure 8 shows r_{eff} vs. M_V of EOs as in Fig. 1 and in addition lines with constant mean surface brightness as defined in Eq. 1. An EO with $r_{\text{eff}} = 10$ pc and $M_V = -5.0$ mag has the same mean surface brightness as an EO with $r_{\text{eff}} = 50$ pc and $M_V = -8.5$ mag. On the other hand, Fig. 8 demonstrates that the trend of the increasing

upper limits of effective radii with increasing total luminosity is not aligned with the lines of constant mean surface brightness. Consequently, the trend cannot be explained as a simple limit of detectability.

The EO catalog and the results presented in Section 3 contain both confirmed EOs and EO candidates. EOs are identified initially in HST images on the basis of an almost round shape and a color consistent with being a GC. The criteria exclude a

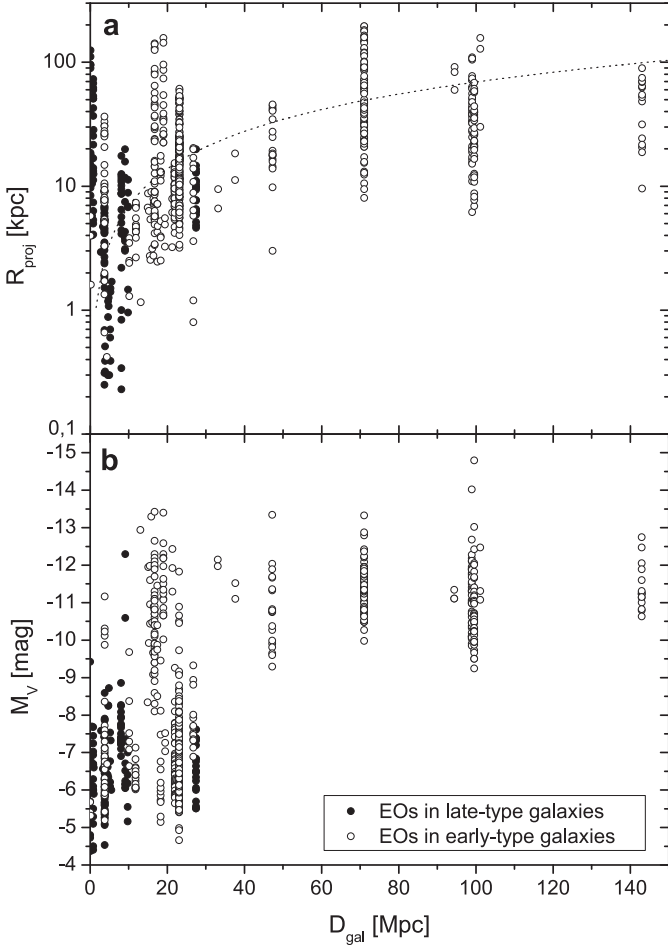


Fig. 7. (a) Projected distances of EOs from their host galaxies are plotted against the distance of the host galaxies. The dotted curve indicates the largest possible projected radius within a single HST ACS image centered on a galaxy at a given distance. (b) Absolute V-magnitudes of EOs are plotted against the distance of the host galaxies.

fair fraction of background galaxies. However, the presence of round background galaxies with the same color as GCs cannot be excluded. Only in the very neighborhood of the Local Group, EOs can be resolved into stars discriminating them from background objects. Consequently, all more distant candidates need to be confirmed by follow-on spectroscopy measuring radial velocities of the objects. As such a procedure is extremely time consuming, only a fraction of the candidate GCs and EOs are observed spectroscopically.

The large extension of EOs leads to significantly lower central surface brightnesses. In terms of central surface brightness, an EO with $r_{\text{eff}} = 10$ pc is roughly a factor of 25 or 3.5 magnitudes fainter than a GC with the same total luminosity, but with $r_{\text{eff}} = 2$ pc. An EO with $r_{\text{eff}} = 30$ pc is already a factor of about 225 or 5.9 magnitudes fainter. Consequently, GCs are typically preferred over EOs during the selection of targets for confirmation, as they are considerably easier to confirm.

From the 813 EOs in the catalog, only 175 EOs were so far spectroscopically confirmed. Figure 9 shows effective radii of confirmed (black) and candidate EOs (grey) as a function of their total V-magnitudes. The confirmed EOs cover basically the same M_V and r_{eff} parameter space as the entire catalog and show the same trend of increasing upper size limits with increasing mass.

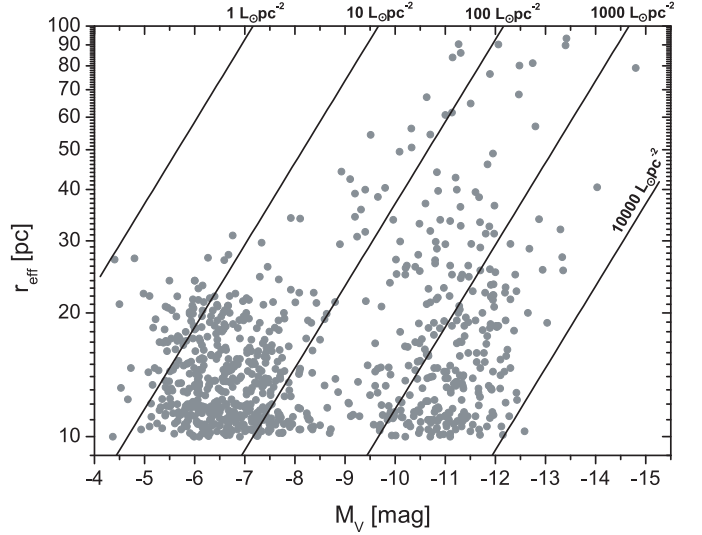


Fig. 8. Effective radii of EOs are plotted against their absolute V-magnitudes (grey circles). The black lines indicate trends of equal mean surface brightnesses of 1, 10, 100, 1000, and 10000 $L_{\odot} \text{pc}^{-2}$.

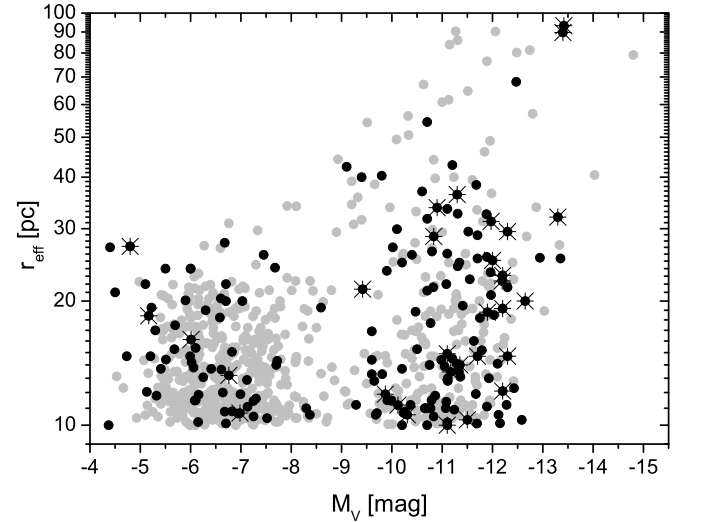


Fig. 9. Effective radii of EOs are plotted against their absolute V-magnitudes. Black circles indicate the 175 confirmed EOs, while grey circles are the 638 EO candidates. The 31 EOs which have a measured dynamical mass are marked by an additional star.

Consequently, the overall distribution of EOs in the r_{eff} vs. M_V space and the trend of increasing upper size-limits with increasing luminosity are not significantly influenced by contaminating background objects.

Figure 10 shows next to the effective radii and total luminosities of EOs also the corresponding parameters of GCs with effective radii smaller than 10 pc. The parameters of the GCs were taken from the same papers used for the EOs (see Sect. 2). The diagram demonstrates that EOs and GCs form a coherent structure in the M_V vs. r_{eff} parameter space.

Figure 11 is a histogram of the effective radii of all star clusters presented in Fig. 10. The largest number of objects is contained in the bin covering effective radii between 2 and 4 pc. For larger effective radii, the number of objects decreases approximately exponentially. Star clusters with effective radii below 6

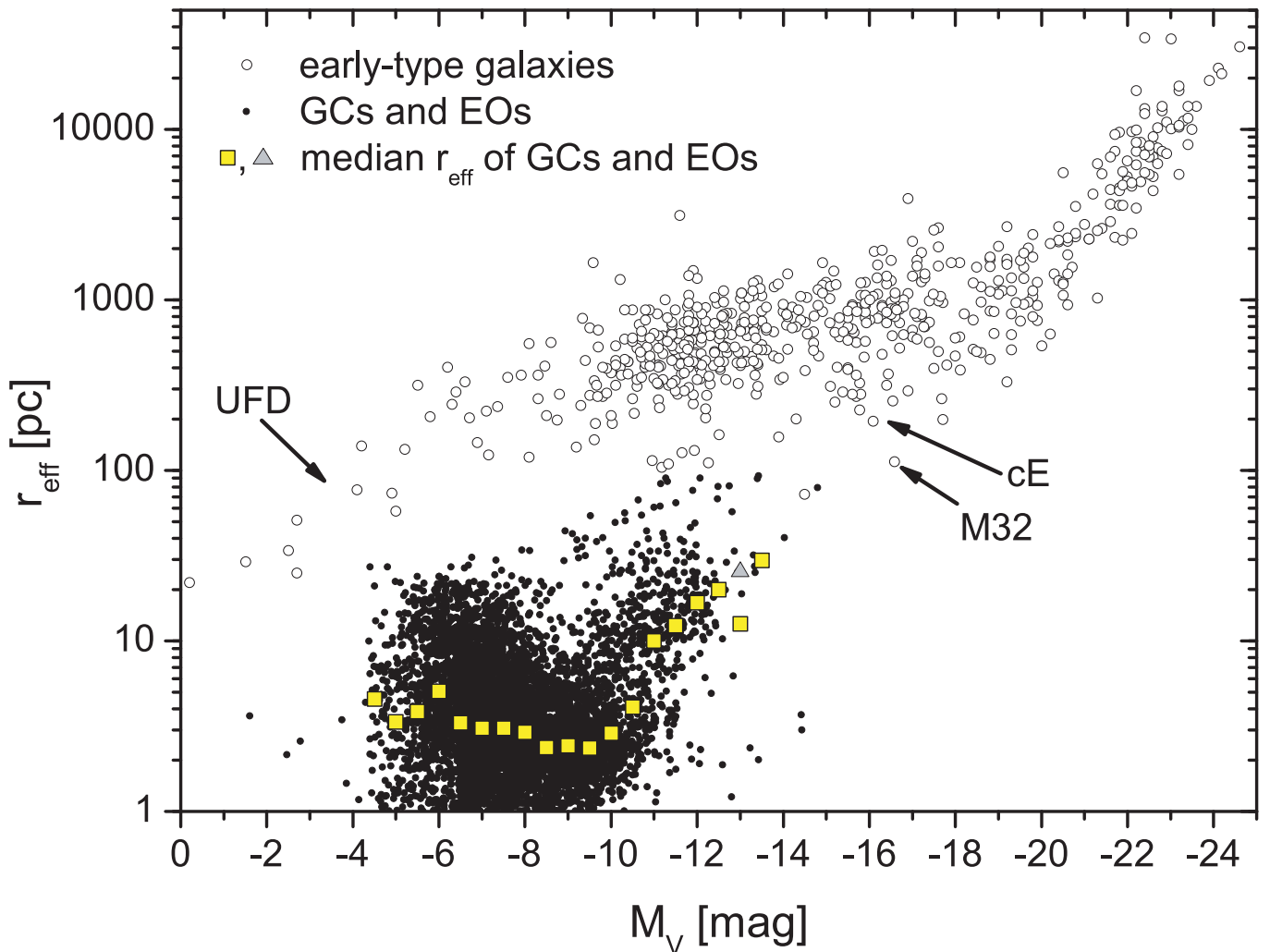


Fig. 10. Effective radii of GCs and EOs are plotted against their absolute V-magnitudes (black circles). The median effective radius per luminosity bin is given as squares. The six exceptionally bright GCs with luminosities between $M_V = -12.5$ and -14.5 mag and effective radii below 4 pc are unconfirmed candidate clusters associated with NGC 4365 (Blom et al., 2012). The grey triangle shows the median effective radius, when these exceptionally bright compact GCs were removed in the bin at $M_V = -13.0$ mag. In addition, early-type galaxies are shown as open circles. Highlighted are the two galaxy types compact ellipticals (cE) with their prototype example M32, and the ultra faint dwarf galaxies (UFD) recently found in the Milky Way.

pc include 80 percent of all objects, while the EOs represent about 10 percent of the objects.

In Fig. 10, the median effective radii per luminosity bin of the combined GC-EO-sample are given as squares. For luminosities fainter than about $M_V = -10.5$ mag, compact clusters with effective radii of a few parsec dominate. With increasing luminosity, EOs start to dominate over GCs leading to an overall trend of increasing effective radii with increasing total luminosity. The median effective radius increases from 10 pc at $M_V = -11.0$ mag to 30 pc at $M_V = -13.5$ mag. At the high-luminosity end, the number of objects is quite low. The low median effective radius at $M_V = -13.0$ mag is due to three very compact candidate GCs in this bin. The removal of these unconfirmed GCs results in a median effective radius that fits the overall trend (grey triangle). While the data show a clear trend of increasing effective radii with increasing luminosity, a tight size-luminosity relation as seen in older publications (e.g. Dabringhausen et al., 2008; Evstigneeva et al., 2008) is no longer existing on the basis of the larger data-set presented in this paper. This result is consistent

with the conclusions of Brodie et al. (2011), which were based on a considerably smaller data-set.

Figure 10 shows next to the GCs and EOs (black circles) also the effective radii and absolute luminosities of early-type galaxies (open circles). We compiled the parameters of the elliptical, dwarf and compact elliptical, and dwarf spheroidal galaxies from Brasseur et al. (2011), Slater et al. (2011), Bell et al. (2011), McConnachie & Irwin (2006), Cappellari et al. (2006), Sharina et al. (2008), Mieske et al. (2005), Huxor et al. (2011b), Belokurov et al. (2010), Misgeld & Hilker (2011), Da Costa et al. (2009), Martin et al. (2008), Price et al. (2009), Geha et al. (2010), Smith Castelli et al. (2008), Smith Castelli et al. (2012), Blakeslee & Barber (2008), and McConnachie (2012). The galaxies span a luminosity range of about 24 magnitudes and a size range of three orders of magnitude.

While the star clusters (GCs and EOs) and the early-type galaxies form both a coherent structure in the M_V vs. r_{eff} parameter space, there is a clear gap between star clusters and galaxies at least in the luminosity interval between $M_V = -6$ mag and

–11 mag. This gap was first discussed by Gilmore et al. (2007). At $M_V = -6$ mag, EOs have effective radii up to about 30 pc, while the dwarf spheroidal galaxies at this luminosity have effective radii between about 100 and 400 pc. In the high-luminosity region at about $M_V = -12$ mag EOs have effective radii up to about 90 pc, while the dwarf galaxies at this luminosity have effective radii between 200 and 1300 pc. Between $M_V = -11$ and -12 mag there are six candidate compact ellipticals from Blakeslee & Barber (2008). They have the same parameters as EOs, but they are slightly larger than 100 pc, which lead to the classification as cEs. As there is no clear distinction between EOs and cEs, these six cEs might as well be very extended EOs.

The ultra faint dwarf galaxies (UFDs), which were recently found around the Milky Way (e.g. Martin et al., 2008; Belokurov et al., 2010), cover the luminosity range between $M_V = 0$ and -5 mag. The detection of large objects with effective radii greater than 20 pc and luminosities fainter than $M_V = -5$ mag is extremely challenging even within the Local Group. While there is no overlap between UFDs and EOs for the Milky Way, a potential overlap of EOs and UFDs for other galaxies cannot be excluded, as neither UFDs nor very faint EOs were within the detection limits of existing surveys.

On the high-luminosity end of the EO distribution, some compact elliptical galaxies have parameters comparable to the most extended EOs. Figure 10 shows two EOs brighter than $M_V = -14$ mag, with effective radii of about 40 and 80 pc (Madrid et al., 2010; Madrid, 2011). However, both are so far unconfirmed candidates that might be background galaxies. The three most luminous, confirmed objects having $M_V \approx -13.4$ mag are VUCD7, UCD3, and HUCD1, which are associated with the central elliptical galaxies of the Virgo Cluster, M87, of the Fornax Cluster, NGC 1399, and the Hydra Cluster, NGC 3311, respectively. In addition, the confirmed object M59cO, which is associated with the giant elliptical galaxy M59, has a luminosity of about $M_V \approx -13.3$ mag. VUCD7 and UCD3 have effective radii of the order of 90 pc, while HUCD1 and M59cO have effective radii of 25 and 32 pc, respectively.

The Coma Cluster compact elliptical galaxy CcGV19b (Price et al., 2009), which has a luminosity of $M_V \approx -14.5$ mag and an effective radius of $r_{\text{eff}} = 72$ pc, is located at a projected distance of 68 kpc to NGC 4874. These parameters could also lead to a classification of CcGV19b as an EO. The observed mass-to-light ratio of about 13 (Price et al., 2009), which is about a factor of three larger than that of VUCD7 and UCD3 (Evstigneeva et al., 2007; Mieske et al., 2008), suggests rather a galactic origin. However, the vast majority of EOs, about 96%, do not have observed velocity dispersions (see Fig. 9), which are needed to estimate a dynamical mass. Consequently, some overlap between EOs and compact elliptical galaxies cannot be excluded.

4.2. EO Luminosity Functions

A common way of parameterization of samples of astronomical objects are luminosity functions. Secker (1992) analyzed compact GCs in the Milky Way and M31 and concluded that their luminosity functions are well represented by so-called Student t_5 functions

$$LF \propto \left[1 + \frac{(M_V - M_{V,\text{TO}})^2}{5\sigma_V^2} \right]^{-3}, \quad (2)$$

where M_V are absolute V-band magnitudes of star clusters, $M_{V,\text{TO}}$ is the turnover of the luminosity function and σ_V is the

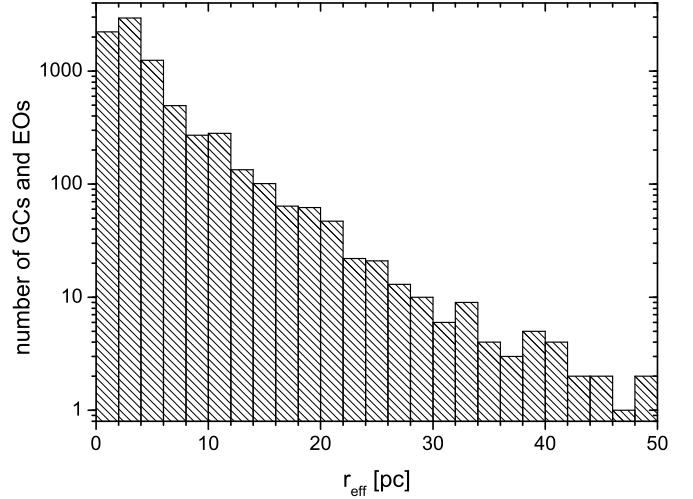


Fig. 11. Histogram of the number of star clusters at different effective radii for all GCs and EOs shown in Fig. 10. The slight increase of numbers at 10 pc is due to the fact that all publications of this paper were selected to contain EOs, but not all of them also include GCs.

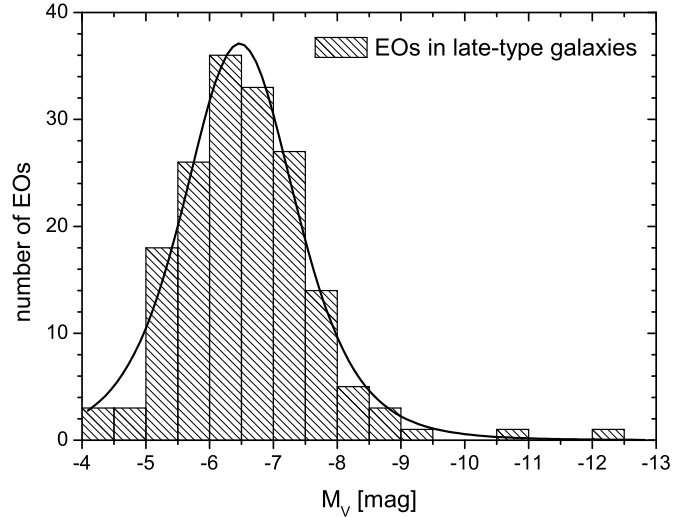


Fig. 12. Histogram of the number of EOs in late-type galaxies at different total V-magnitudes. The black line represents a fitted t_5 luminosity function.

dispersion of the t_5 function. For compact GCs, the turnover of the luminosity function, $M_{V,\text{TO}}$, is very constant for various types of galaxies, making it a reasonable distance estimator (see Rejkuba, 2012, and references therein). The mean turnover luminosity for the Milky Way and 18 nearby galaxies is $M_{V,\text{TO}} = -7.66 \pm 0.09$ mag.

4.2.1. EOs in Late-Type Galaxies

A histogram of the number of EOs at different total luminosities of late-type galaxies is shown in Fig. 12. A fit of the luminosity function according to Eq. 2 is added. The turnover of the luminosity function is $M_{V,\text{TO}} = -6.47 \pm 0.03$ mag and the dispersion of the t_5 function is $\sigma_V = 0.91 \pm 0.03$ mag. The peak of the EO luminosity function is about one magnitude fainter than the typical peak of the GC luminosity function.

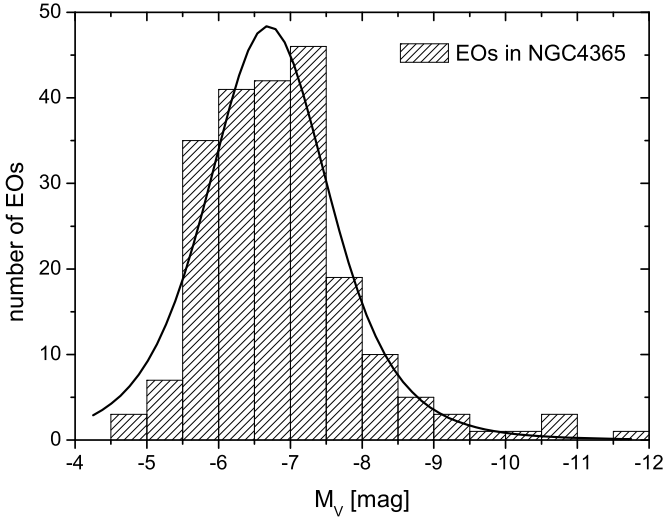


Fig. 13. Histogram of the number of EOs in the elliptical galaxy NGC4365 at different total V-magnitudes. The black line represents a fitted t_5 luminosity function.

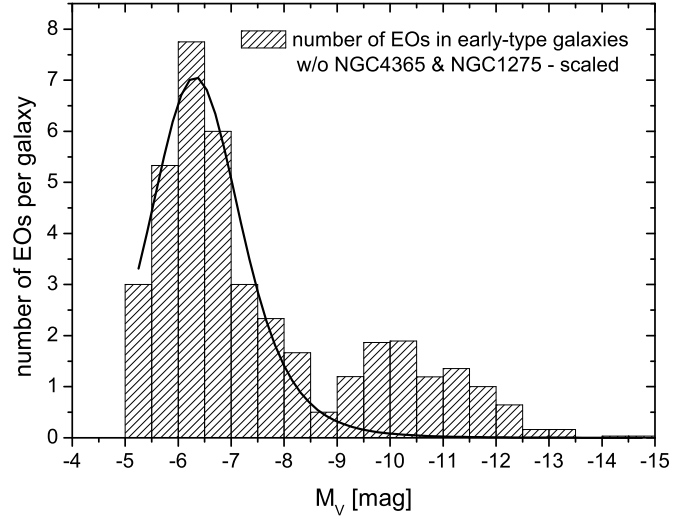


Fig. 15. Histogram of the normalized number of EOs in early-type galaxies except for the large EO samples of NGC4365 and NGC1275 at different total V-magnitudes scaled by the number of galaxies having observations at the individual bins. The black line represents a fitted t_5 luminosity function.

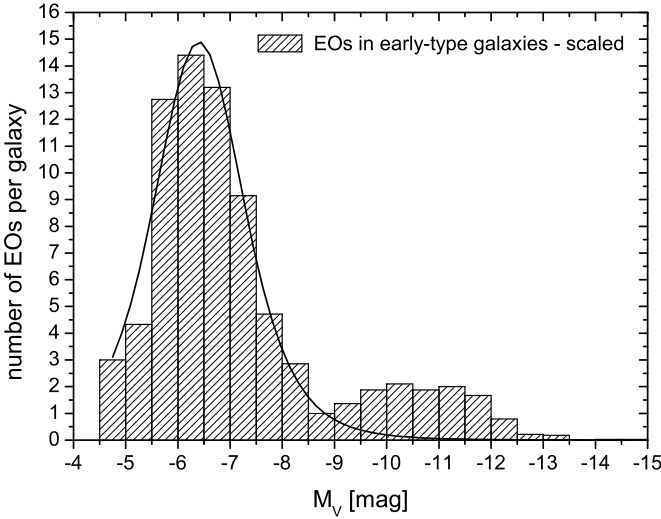


Fig. 14. Histogram of the normalized number of EOs in early-type galaxies at different total V-magnitudes scaled by the number of galaxies having observations at the individual bins. The black line represents a fitted t_5 luminosity function.

For the histogram in Fig. 12 all 171 EOs associated with late-type galaxies are used. As discussed in Section 4.1, only a fraction of EOs were confirmed by follow-on spectroscopy. Consequently, it cannot be excluded that some background galaxies modified the exact result of the luminosity function. The number of confirmed EOs in late-type galaxies is 43. The mean total luminosity of the 43 EOs is $M_V = -6.40$ mag. Considering the low number of objects, this value is quite close to the fitted value for all candidate EOs, indicating that the EOs in late-type galaxies indeed have a fainter peak of the luminosity function than compact GCs.

Considering the very low surface brightness of faint and extended EOs (see Sect. 4.1), a fair fraction of very extended and faint EOs is most likely below the detection limit of extragalactic surveys. The true turnover of the EO luminosity function might therefore be at even lower luminosities.

4.2.2. EOs in Early-Type Galaxies

Figure 3 shows that EOs in early-type galaxies show a bimodal distribution which peaks at about $M_V = -6.5$ mag and -11.0 mag and has a clear minimum between -8.5 and -9 mag. On the other hand, Figure 7b demonstrates that for a large fraction of early-type galaxies only high-luminosity objects were considered. This is partly due to detection limits especially at large distances, but also due to the fact that since the discovery of UCDS in the Fornax Cluster by Hilker et al. (1999) and Drinkwater et al. (2000), much effort has been made to detect and to analyze EOs brighter than about $M_V = -10$ mag, while fainter EOs were neither in the focus of UCD studies nor in those investigating GCs.

A number of GC surveys applied size limits to reduce the contamination of background galaxies. For instance, the GC surveys covering 100 galaxies of the Virgo Cluster (Jordán et al., 2005) and 43 galaxies of the Fornax Cluster (Masters et al., 2010) applied a size limit of $r_{\text{eff}} < 10$ pc to reduce the contamination by background galaxies. As a side effect, they excluded also all EOs from their GC catalogs.

The very different approaches for objects with low and high luminosities have a significant influence on the luminosity function. One example is the galaxy M85 of the Virgo Cluster. Four EOs are found with luminosities brighter than $M_V = -8.5$ mag (Haşegan et al., 2005; Chies-Santos et al., 2011). Peng et al. (2006) used the same Virgo Cluster survey data as Jordán et al. (2005) to search for diffuse star clusters and concluded that the galaxy M85 has about 30 EOs with luminosities between $M_V = -5.5$ and -8.5 mag. While the low luminosity objects would dominate for this galaxy, our catalog contains only the four bright M85 EOs of Haşegan et al. (2005) and Chies-Santos et al. (2011) as Peng et al. (2006) have not published a catalog of their EOs. In the same field of view Jordán et al. (2005) found 211 compact GCs in M85. For this specific galaxy, the EOs would add about 15% to the GC sample.

Another example is the giant elliptical galaxy NGC 4365, which was covered by eight HST ACS fields (Blom et al., 2012).

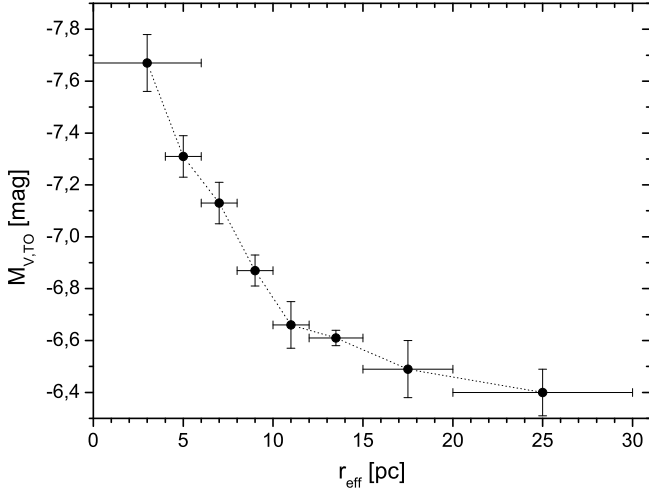


Fig. 16. Turnover of the luminosity function, $M_{V,\text{TO}}$, of GC and EOs plotted as a function of the effective radius. The error bars in r_{eff} indicate the individual bin-sizes, the error bars in $M_{V,\text{TO}}$ show the statistical error of the fit of the luminosity function to the data.

Seven HST ACS fields provide a very good coverage of the inner 35 kpc of the galaxy while the last field pointed to the halo delivering clusters with projected distances between about 40 and 60 kpc. Blom et al. (2012) found in total 2038 GC and 217 EO candidates. For this galaxy, EOs add about 10 percent to the GC sample. Only 5 of the 217 EOs are brighter than $M_V = -10$ mag, 19 EOs have a luminosity between $M_V = -8$ and -10 mag, and 148 EOs have one between $M_V = -6$ and -8 mag. Again, the number of low-luminosity EOs is significantly larger than the number of bright EOs. The EO candidates of NGC4365 form the largest EO sample of an elliptical galaxy. Figure 13 shows the histogram of the number of EO candidates of NGC4365 as a function of luminosity. The black line shows the corresponding luminosity function having a turnover luminosity of $M_{V,\text{TO}} = -6.69 \pm 0.07$ and a dispersion of the t_5 function of $\sigma_V = 0.88 \pm 0.07$ mag. The turnover luminosity is at slightly brighter luminosities as for the late-type galaxies.

In their central HST field, Blom et al. (2012) found 681 compact clusters and 30 EOs, i.e. the EOs add about 4.4% to the GC sample in the central region of NGC 4365. For the 100 Virgo galaxies Jordán et al. (2005) found in single HST fields centered on the individual galaxies in total 12763 compact GCs. An EO fraction of 5% would yield for these 100 galaxies an EO population of 638 EOs, which is about ten times the number of high luminosity objects in our catalog associated with these Virgo Cluster galaxies.

Consequently, an interpretation of the bimodal luminosity distribution needs to take into account the varying number of galaxies building the sample at each luminosity bin. Only seven early-type galaxies have observations of EOs fainter than $M_V = -8.5$ mag and only four galaxies have observations of EOs fainter than $M_V = -6.5$ mag. For EO luminosities from $M_V = -8.5$ mag to -10.5 mag, the number of observed galaxies increases from 9 to 20. EOs brighter than $M_V = -10.5$ mag were observed in 33 galaxies.

Figure 14 takes the varying number of galaxies into account, i.e. the number of EOs in each bin is divided by the number of galaxies contributing to this luminosity bin. The second peak at high luminosities has decreased considerably, but it has not

entirely vanished, demonstrating that the large number of high-luminosity EOs associated with the most luminous galaxies is not a simple size-of-sample effect. A fit of the luminosity function according to Eq. 2 is added to Fig. 14. The peak of the luminosity function is at $M_{V,\text{TO}} = -6.40 \pm 0.06$ mag and the dispersion of the t_5 function is $\sigma_V = 0.89 \pm 0.07$ mag. The values change only slightly to $M_{V,\text{TO}} = -6.40 \pm 0.05$ mag and $\sigma_V = 0.87 \pm 0.06$ mag when the high-luminosity tail (i.e. objects brighter than $M_V = -9$ mag) is excluded from the fit.

The EO sample of early-type galaxies is dominated by the two galaxies NGC4365 and NGC1275, which have 217 and 84 EO candidates, respectively. In order to verify that the results for early-type galaxies are not biased towards these two galaxies, we have repeated the exercise of scaling the number of objects per luminosity bin by the number of relevant galaxies excluding NGC4365 and NGC1275 from the sample. Figure 15 shows the resulting histogram and a fitted luminosity function having $M_{V,\text{TO}} = -6.32 \pm 0.10$ mag and $\sigma_V = 0.89 \pm 0.12$ mag. The results of the sample without NGC4365 and NGC1275 agree well with the results of the entire EO sample of early-type galaxies.

The results for early-type galaxies are very similar to the results from late-type galaxies. The main difference between the luminosity functions is the tail of high-luminosity objects associated with early-type galaxies.

Mieske et al. (2012) studied a sample of confirmed GCs and UCDs to address the question whether there is an over-population of UCDs with respect to compact GCs. They concluded that the number of UCDs is consistent with a continuation of the GC luminosity function towards bright magnitudes. In this paper, we demonstrate that there is an over-population of bright EOs if compared with the EO luminosity function. While the Mieske et al. (2012) sample is well defined in the sense that all objects were spectroscopically confirmed, most of them have no measured size. They used all UCDs irrespective of their size and compared the number of UCDs with the GC luminosity function which has a turnover luminosity that is about one magnitude brighter than the EO luminosity function. In addition, the number of GCs is about 10 times larger than the number of EOs. Consequently, the results of Mieske et al. (2012) cannot easily be compared with our results as the samples are largely independent from each other. Larger EO and GC samples of a number of early type galaxies covering the entire luminosity range from $M_V = -4$ to -14 mag are needed to answer the question whether there is a general overpopulation of bright EOs in early-type galaxies or whether it is a specific feature seen only in special environments.

4.2.3. Trends of the turnover luminosity with effective radius

In the previous sections, we concluded that EOs in early and late-type galaxies have basically the same turnover of the luminosity function, which is about one magnitude fainter than that of compact GCs.

In this section, we explore the trend of the turnover luminosity with increasing effective radii. In order to increase the number of objects per r_{eff} -bin, we combine the data for GCs and EOs of early and late-type galaxies. We exclude the brightest objects in the UCD regime to avoid the second peak as seen in Figs. 3 and 14 and focus on objects fainter than $M_V = -9$ mag.

For the compact GCs with effective radii below 6 pc, we derive a turnover of the luminosity function of $M_{V,\text{TO}} = -7.67 \pm 0.11$ mag, which is in very good agreement with the mean turnover luminosity for the Milky Way and 18 nearby galaxies, $M_{V,\text{TO}} = -7.66 \pm 0.09$ mag (Rejkuba, 2012).

Figure 16 shows the trend of the turnover luminosity as a function of the effective radius. The turnover luminosity decreases continuously from $M_{V,TO} = -7.67$ mag to $M_{V,TO} = -6.66$ mag at the r_{eff} -bin between 10 and 12 pc. For larger effective radii, the turnover luminosity decreases considerably slower to values of $M_{V,TO} = -6.40$ mag at the r_{eff} -bin between 20 and 30 pc.

On the basis of the available data, we conclude that the turnover of the luminosity function depends significantly on the effective radii of star clusters and that the slope of the varying $M_{V,TO}$ is steeper for GCs than for EOs.

However, the edge in the luminosity function at $M_V = -5.0$ mag for late-type and at $M_V = -5.5$ mag for early-type galaxies indicates that the samples are fairly incomplete at very low luminosities. The true turnover of the EO luminosity function is therefore expected to be at even lower luminosities, which might lead to a steeper slope in the EO regime. Considerably larger and more complete data-sets especially at low-luminosities, consisting of confirmed star clusters, are necessary to confirm the trend of the luminosity functions from GCs to EOs as shown in Fig. 16 and to substantiate the idea that this trend is a general feature of GCs and EOs in early- and late-type galaxies.

4.3. Spatial Distribution of EOs

In the Milky Way, the 11 EOs have galacto-centric distances between 16 and 125 kpc with a median distance of 72 kpc. In contrast, the GCs of the Milky Way are at considerably lower distances. The median distance of the GCs is 4.8 kpc. For M31 five out of 20 EOs have projected distances smaller than 10 kpc and 11 EOs have projected distances larger than 20 kpc (Peacock et al., 2009; Huxor et al., 2008). The two EOs associated with M33 have projected distances of 12.5 and 28.4 kpc (Stonkutė et al., 2008; Huxor et al., 2009).

The most serious constraint of EO catalogs of galaxies outside the Local Group is the very limited field of view of the HST ACS instrument, as EOs at large distances from the Galaxy can only be spatially resolved by HST. The field of view of the ACS instrument is $202''$ and the pixel size is $0.05''$.

The dotted curve in Fig. 7a indicates the largest possible projected radius of a single HST ACS image centered on a galaxy at a given distance. It visualizes the area covered by one Hubble field. At small distances a couple of HST ACS fields are necessary to scan a galaxy for EOs, whereas at large distances the galaxy and part of the halo are completely covered by one HST ACS field.

At the distance of the Whirlpool Galaxy M51 of about 8 Mpc, the field of view of $202''$ and the pixel size of $0.05''$ correspond to 7.8 kpc and 2 pc, respectively. While the pixel size is well suited to resolve EOs, a number of ACS images are needed to cover the entire galaxy. Figure 17 shows an image of the Digitized Sky Survey 2 (DSS2¹) of M51 and the area covered by the mosaic of six ACS images used by Hwang & Lee (2008) to find EOs in M51, demonstrating that even six HST ACS images do not cover the entire stellar body of the interacting galaxy pair.

The HST mosaic of M51 covers an area of $15.7 \text{ kpc} \times 23.6 \text{ kpc}$. This coverage is well suited to detect EOs related to the stellar bodies of the two galaxies and EOs in the lower halo. While halo EOs at considerably larger distances from their host galaxies might be found by chance in projection to the main body of

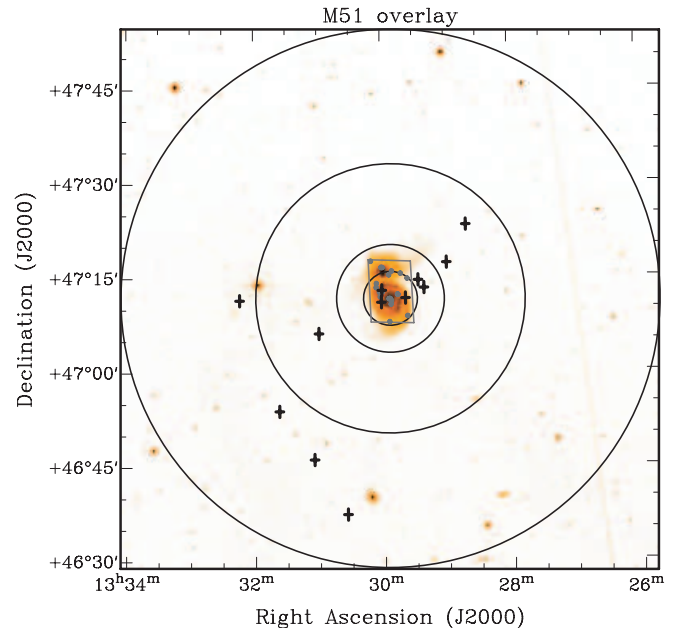


Fig. 17. M51 EOs (grey dots) overlaid on a Digitized Sky Survey 2 (DSS2) image of M51. The grey lines indicate the size of the HST mosaic of 6 ACS images used by Hwang & Lee (2008) to find EOs in M51. The black circles indicate projected distances from M51 of 10, 20, 50, and 100 kpc. For comparison, the projected position of the Milky Way EOs, if the Milky Way would be seen face-on at the distance and the position of M51, are added as black crosses.

the host galaxy, the probability is relatively low. Considering a line-of-sight of ± 100 kpc, the volume covered by the HST mosaic is $15.7 \times 23.6 \times 200 \text{ kpc}^3$, or $7.4 \cdot 10^4 \text{ kpc}^3$. In contrast, the volume with a radius of 100 kpc, which would enclose the EOs, is $\frac{4}{3}\pi 100^3 \text{ kpc}^3$ or $4.2 \cdot 10^6 \text{ kpc}^3$. The HST mosaic of six ACS images covers less than 2 percent of the volume expected to contain EOs.

Figure 17 shows for comparison also the location of the Milky Way EOs, if the Milky Way would be seen face-on at the distance and the position of M51. The six most distant EOs of the Milky Way have large galacto-centric distances between 70 and 125 kpc, or projected distances between 41 and 84 kpc in Fig. 17. This figure demonstrates that only 3 of 11 EOs would be located within the HST mosaic. Consequently, also a number of EOs of M51 are expected to have considerably larger projected distances beyond the currently covered survey area.

In addition to EOs located in galactic halos, Larsen & Brodie (2000) and Brodie & Larsen (2002) have discovered a population of EOs co-rotating with the disk of the lenticular galaxy NGC 1023. These so-called faint fuzzies have similar structural parameters as halo EOs and are therefore not easily distinguishable from halo EOs projected onto the disk on the basis of imaging data alone. A fair fraction of EOs found in extragalactic surveys - especially those covering only the disk regions like the M51 survey (Hwang & Lee, 2008) - might therefore be associated with the disks and not the halos of these galaxies.

The Hydra Cluster is located at a distance of about 47.2 Mpc. Misgeld et al. (2011) searched with ground based telescopes for massive star clusters in Hydra and detected and spectroscopically confirmed 118 objects with total V-band luminosities between $M_V = -9.7$ and -13.3 mag and projected distances between 3 and 300 kpc. The median projected distance is 44 kpc.

¹ The Digitized Sky Survey data used in this paper have been taken from the ESO Archive, see <http://archive.eso.org/dss/dss>

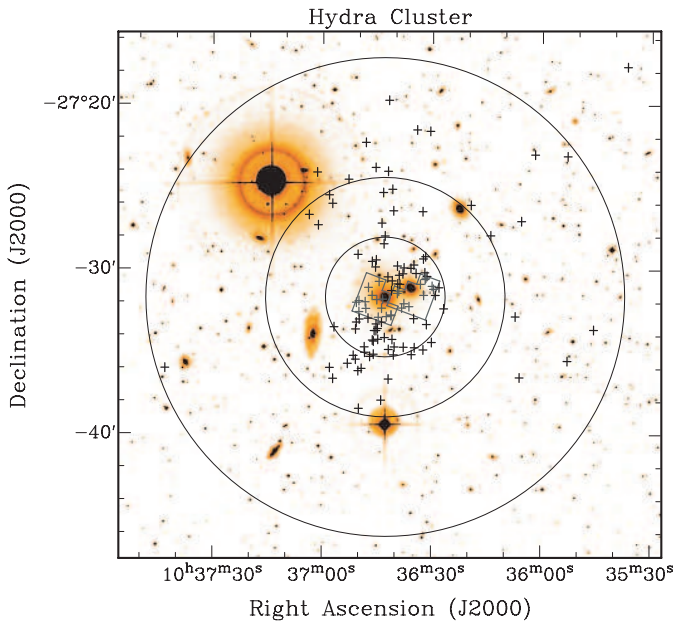


Fig. 18. Spectroscopically confirmed star clusters (crosses) of the Hydra Cluster (Misgeld et al., 2011) overlaid on a DSS2 image of the Hydra Cluster. Only those clusters which are located within the two HST WFPC2 fields (marked by grey lines) have measured sizes. The black circles indicate projected distances from the central galaxy NGC3311 of 50, 100, and 200 kpc.

Only 26 of the 118 stellar objects are located within two HST WFPC2 fields (see Fig. 18). 19 of the 26 objects are EOs and the remaining 7 objects have effective radii between 8 and 10 pc. It is expected that also a large fraction of the remaining 92 objects in the outer halo are EOs. In addition, Fig. 7 of Misgeld et al. (2011) demonstrates that star clusters are not uniformly distributed in the halo. While some halo fields contain several UCDS, other fields have no UCDS at all. Consequently, random samples of small fields in a halo cannot be used to extrapolate to the entire population.

Another example is the giant elliptical galaxy NGC 4365, which was covered by eight HST ACS fields (Blom et al., 2012). Seven HST ACS fields provide a very good coverage of the inner 35 kpc of the galaxy. In their central HST field, Blom et al. (2012) found 681 GC and 30 EO candidates, while the six HST fields surrounding the central field have on average 216 GCs and 26 EOs. The results demonstrate that the number density of compact clusters decreases rapidly towards larger projected distances while the number of EOs per HST field is almost constant. In addition, Blom et al. (2012) searched for star clusters outside the HST fields with ground based telescopes and concluded that the cluster system extends out to projected radii of about 135 kpc and contains about three times the number of clusters as the HST fields. Consequently, there are several hundreds of EOs expected in the halo of NGC 4365 outside the HST fields.

The three examples M51, NGC4365 and the Hydra Cluster are typical for the entire sample of galaxies with EOs. The vast majority of the studied galaxies have a reasonable coverage of the main stellar body, but a very poor coverage of the halo by HST observations. Only very distant galaxies like the elliptical galaxy ESO 325-G004 in the galaxy cluster Abell S0740 at a Galactic distance of 143 Mpc are well covered (including the halo) by one HST ACS field. However, the pixel size of the HST

ACS of $0.05''$ corresponds to a linear scale of about 35 pc at this distance, which is too coarse to resolve rather compact EOs.

A considerably larger fraction of the halos of early and late-type galaxies needs to be covered by HST observations to allow for a conclusive view on the spatial distribution of EOs and possible differences between early and late-type galaxies.

4.4. An EO Formation Scenario

Phillipps et al. (2001) interpreted the high-luminosity EOs as a new type of galaxy and reflected this interpretation in the name “ultra-compact dwarf galaxy” (UCD). Bekki et al. (2001, 2003) suggested that UCDS are the remnants of dwarf galaxies which lost their dark matter halo and all stars except for their nucleus. Next to the interpretation as a galaxy, UCDS were also considered as high-mass versions of normal GCs (Mieske et al., 2002), or as merged massive complexes of star clusters (Kroupa, 1998; Fellhauer & Kroupa, 2002a; Brüns et al., 2011). In this paper, we will focus on the latter, i.e. the star cluster origin where EOs are the end products of merged star clusters.

A few decades ago ‘young massive star clusters’ (YMCs) were found with globular cluster-like properties. YMCs are found in all types of gas-rich galaxies and constitute a common class of star clusters. The definition of YMCs is rather author dependent. We adopt the definition of Whitmore (2003) who defined ‘young’ as having an age less than 500 Myr and ‘massive’ as having masses ranging from $10^3 M_{\odot}$ to $10^8 M_{\odot}$. Individual YMCs were analyzed in detail by Bastian et al. (2006b), Mengel et al. (2008), and Bastian et al. (2009). The combined data-set of the three publications demonstrates that the median size of YMCs in the mass range between $10^5 M_{\odot}$ and $10^6 M_{\odot}$ is about 4 pc. YMCs with masses of a few times $10^7 M_{\odot}$ have only been observed in strong starburst environments like for example in the interacting galaxy NGC 6745 (de Grijs et al., 2003) and the late-stage merger galaxies NGC 7252 (Maraston et al., 2004) and Arp 220 (Wilson et al., 2006).

Observations have shown that YMCs are often not isolated, but are part of larger structures called CCs (e.g. Bastian et al., 2006a). The CCs contain few to hundreds of YMCs spanning up to a few hundred parsecs in diameter. The mass of a CC is the sum of its YMC constituents. Little is known about the detailed distribution of the individual star clusters inside a CC and about their velocity distribution, largely because the existence of CCs had not been realized fully until only very recently. However, the observations show that most CCs have a massive concentration of star clusters in their centers and a couple of isolated star clusters in their vicinity.

Examples for CCs are the knots of the interacting galaxies NGC 4038 and NGC 4039 at a distance of about 20 Mpc, aka the Antennae, which have typical masses of the order of $M_{\text{knot}} = 10^6$ to $10^7 M_{\odot}$ and sizes of a few hundred parsecs (Whitmore et al., 2005). The knots typically consist of about 30 young massive star clusters with masses greater than $10^4 M_{\odot}$ and about 60 lower-mass clusters (Whitmore et al., 2010). Whitmore et al. (2005) found that the cluster to cluster velocity dispersion in the knots is small enough to keep them gravitationally bound leading to merging of clusters in the central region of the knots. The collision between the two gas-rich Antennae galaxies triggered the formation of super giant molecular complexes with masses up to $9 \cdot 10^8 M_{\odot}$ (Wilson et al., 2003). It is expected that these super massive gas clouds will be the birth sites of very massive CCs. Some starburst galaxies like for example Arp 220 at a distance of 77 Mpc host YMCs/CCs as massive as $10^7 M_{\odot}$ with ages less than 10 Myr (Wilson et al., 2006). Arp 220 also represents

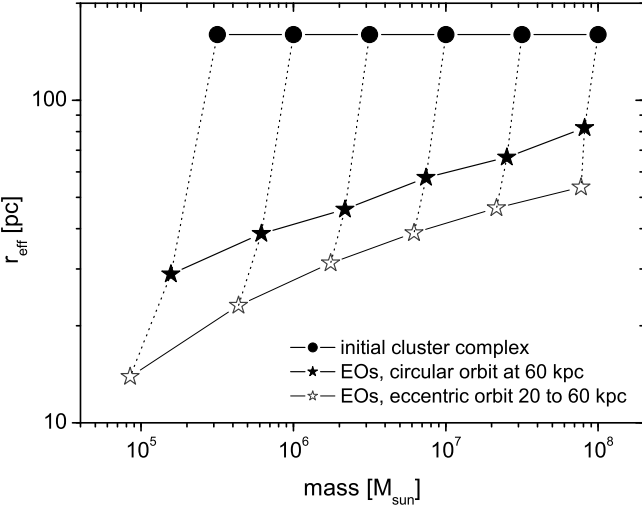


Fig. 19. Diagram of r_{eff} as a function of mass for the modeled merger objects on a circular orbit at 60 kpc (black stars) and on an eccentric orbit between 20 and 60 kpc (open stars) after a dynamical evolution of 5 Gyr (see Brüns et al., 2011, for details). For comparison, the parameters of the initial CCs (black circles) are included. The initial CCs are connected with the corresponding merger objects by dotted lines.

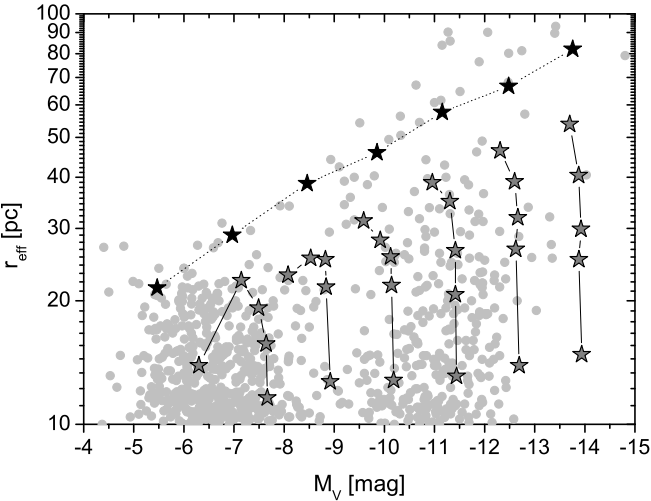


Fig. 20. Diagram of r_{eff} as a function of the total luminosity of the observed EOs (grey circles) and the modeled merger objects (stars) from Brüns et al. (2011). Merger objects on eccentric orbits between 20 and 60 kpc are plotted in dark grey. Objects with the same initial CC mass but different initial CC effective radii between 10 and 160 pc are connected by black lines. Merger objects on a circular orbit at 60 kpc and an initial effective radius of the CC of 160 pc are plotted as black stars connected by dotted lines.

two colliding spiral galaxies, but already in the end phase of the merging process. The late-stage merger galaxy NGC 7252 hosts a very massive star cluster (W3) with an age between 300 and 500 Myr. It has a mass of about $8 \cdot 10^7 M_{\odot}$ and an effective radius of $R_{\text{eff}} = 17.5$ pc (Maraston et al., 2004). From its structural parameters W3 may be classified as a young version of a UCD. The young age of W3 precludes an origin as a remnant nucleus of a stripped dwarf galaxy. W3 may instead have evolved from a CC by merging of its constituent star clusters (Fellhauer & Kroupa,

2005). Another example is the Tadpole galaxy (UGC 10214), which is a disrupted barred spiral galaxy at a distance of about 130 Mpc. The galaxy shows a long tidal tail of stars, which hosts also some CCs. The most luminous and largest CC in the tail has a mass of the order $M_{\text{CC}} = 10^6 M_{\odot}$, an effective radius of $r_{\text{eff}} = 160$ pc, a cut-off radius of about $r_{\text{cut}} = 750$ pc and it is located at approximately 60 kpc from the center of the galaxy (Tran et al., 2003).

Since galaxy-galaxy mergers are anticipated to have been more common during early cosmological times it is expected that star formation in CCs has been a significant star formation mode during this epoch. Indeed, the preponderance of clumpy galaxies (Elmegreen, 2007, and references therein) indicates that early gas-rich galaxies went through an epoch of profuse CC formation. Bournaud et al. (2008a) performed high-resolution modeling of a galaxy interaction that lead to a merger remnant comparable to an elliptical galaxy. In these models, super star clusters with masses of a few $10^7 M_{\odot}$ and sizes up to about 150 pc formed in the halo of this merger remnant. Bournaud et al. (2008b) demonstrated that these star clusters are gravitationally stable.

The dynamical evolution of CCs with a large range of initial configurations and on various orbits was studied in a number of publications (e.g. Kroupa, 1998; Fellhauer & Kroupa, 2002a,b, 2005; Bekki et al., 2004; Brüns et al., 2009; Brüns & Kroupa, 2011; Brüns et al., 2011). These studies demonstrated that the merging star cluster scenario provides a mechanism for the formation of EOs.

In a previous paper (Brüns et al., 2011), we varied sizes and masses of the modeled CCs covering a matrix of 5×6 values with effective radii between 10 - 160 pc and CC masses between $10^{5.5} - 10^8 M_{\odot}$. These models were placed on eccentric orbits between 20 and 60 kpc and were simulated over a period of 5 Gyr². In addition, models with CCs having effective radii of 160 pc were placed on a circular orbit at a distance of 60 kpc. Figure 19 shows the location of the initial CCs having $r_{\text{eff}} = 160$ pc and the corresponding modeled merger objects on the eccentric and the circular orbit after 5 Gyr of evolution. Due to the merging process and the external tidal field, the final masses and effective radii of the merger objects are considerably lower than those of the initial CCs. The comparison between the eccentric and the circular orbits demonstrates that the tidal field plays a crucial role for the final parameters of the merger objects.

Figure 20 shows effective radii and estimated total V-band luminosities of the models of Brüns et al. (2011) using a mass-to-light ratio of 3 and the parameters of the 813 EOs as given in Fig. 1. Figure 20 demonstrates that the observed and simulated EOs cover the same parameter space and show the same trend of increasing effective radii with increasing luminosity.

The merged cluster scenario also helps to understand the difference between the mass function of YMCs, which is a power-law with a slope of -2 and the GC/EO luminosity functions, which have a bell-shaped function as given in Eq. 2. Most publications focused on the destruction of low-mass clusters (for a recent review see Portegies Zwart et al., 2010, and references therein). The merged cluster scenario predicts that dozens of low-mass YMCs merge to form one EO. As EOs add approximately 10% to the number of GCs, it is expected that the total number of low-mass clusters needed to build up the EOs is larger than the actual number of remaining GCs. Consequently,

² Brüns & Kroupa (2011) demonstrated that the structural parameters of the merger objects change only marginally after the merging process is concluded after a few Gyr.

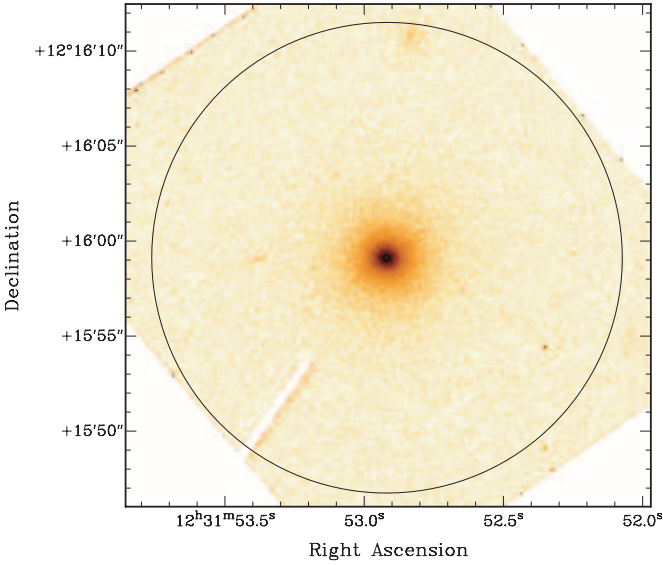


Fig. 21. High resolution HST ACS image of VUCD7 in the F606W filter. The black circle has a projected radius of 1 kpc indicating the extent of the surface brightness profile shown in Figure 22.

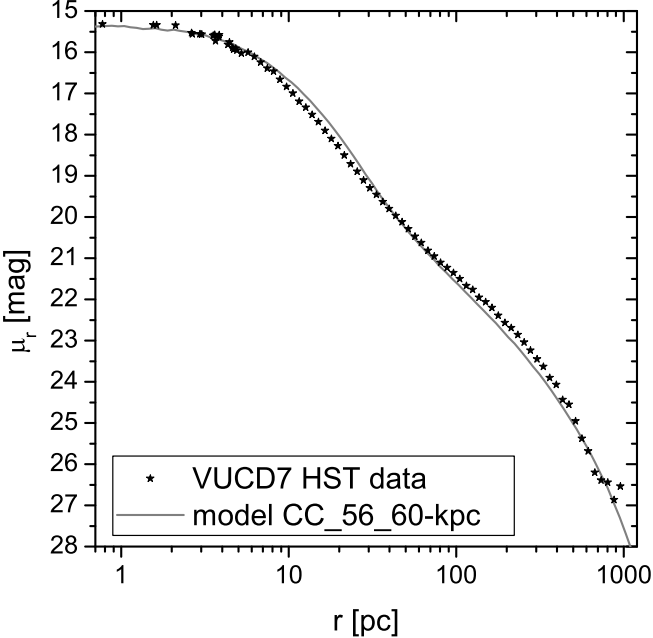


Fig. 22. Surface brightness profile compiled from archival HST ACS data (black stars) of the EO VUCD7 and the surface brightness profile of model CC_56_60-kpc (grey line) from Brüns et al. (2011) using a mass-to-light ratio of 2.8. The model and the observed EO show a very similar two-component or “core-halo” structure.

the merged cluster scenario predicts that a fair fraction of the low-mass YMCs evolve via merging into EOs modifying the original power-law luminosity function.

YMCs and CCs with masses below $M = 10^6 M_{\odot}$ have been observed in all types of galaxies containing sufficient amounts of gas to form star clusters, while high-mass YMCs and CCs ($M \gtrsim \text{few} \times 10^6 M_{\odot}$) were so far only observed in major merger events like the Antennae, Arp 220, or NGC 7252, which may be in the process of becoming elliptical galaxies. This explains the different EO luminosity functions for late-type and early-type

galaxies: only the major interactions that create the early-type galaxies build CCs massive enough to form the EOs considerably brighter than about $M_V = -10$ mag.

The evolution of low-mass EOs in a weak gravitational environment has also been studied by Hurley & Mackey (2010), who performed direct N-body models of extended low-mass star clusters incorporating a stellar mass function and stellar evolution. Internal evolution processes of the star clusters lead to considerably larger effective radii compared to the initial values. They concluded that extended star clusters with an initial mass of $5.8 \cdot 10^4 M_{\odot}$ are sufficiently stable to survive a Hubble-time in a weak gravitational field environment.

Murray (2009) addressed the question why compact star clusters are absent in the high-mass regime, i.e. at masses larger than few $10^6 M_{\odot}$. Murray (2009) modelled proto-clusters and found that high-mass clusters become optical thick to infra-red radiation leading to a modified initial mass function of the cluster stars, to a larger mass-to-light ratio, and to considerably larger sizes of the proto-clusters. While the idea of optically thick proto-clusters explains the absence of compact clusters in the high-mass regime, it cannot explain the existence of EOs over the large observed mass-range.

An alternative formation scenario for high-mass EOs is the galaxy threshing scenario, where nucleated dwarf galaxies loose, during a heavy interaction with a larger galaxy, almost all stars of the main body except for the nucleus (Bekki et al., 2001). This formation scenario connects EOs with compact elliptical galaxies like M32, as this rare species of compact galaxy is also expected to be the end-product of an interaction that stripped the bigger part of a formerly larger galaxy. Bekki et al. (2003) performed numerical simulations to demonstrate that nucleated dwarf galaxies can indeed evolve into EOs if they are on a highly eccentric orbit. However, these studies on the threshing scenario focussed on the UCD regime. So far, it was not demonstrated that the threshing scenario is able to reproduce also low-mass EOs.

According to Bekki et al. (2003), a two-component “core-halo” surface brightness profile is a major prediction of the galaxy threshing scenario, where the core is the former nucleus and the halo is the remnant of the main body of the former galaxy.

Three of the four most luminous confirmed EOs, i.e. VUCD7, UCD3, and M59cO, show a clear two-component or core-halo surface brightness profile. Following the results of Bekki et al. (2003), this kind of structure was used as evidence for a galactic origin of UCDS (e.g. Haşegan et al., 2005; Chilingarian & Mamon, 2008; Norris & Kannappan, 2011). While UCD3 is largely overlapping with a background spiral galaxy and M59cO has a projected distance to M59 of only 9 kpc, the most extended and most luminous of the three objects, VUCD7, is located about 83 kpc from M87 and has neither disturbing foreground nor background objects in its vicinity. Figure 21 shows an HST ACS high-resolution image in the F605W band³. The HST data allow to compile a surface brightness profile out to large projected radii of about 1 kpc.

Figure 22 shows the surface brightness profile of VUCD7 compiled from the archival HST ACS data presented in Fig. 21 using a median filter for the radial bins to exclude faint emission from possible foreground or background objects. The observed profile of VUCD7 shows a clear two-component structure. Whereas most of the models from Brüns et al. (2011) show a sin-

³ The HST ACS image of VUCD7 was taken from the Hubble Legacy Archive, see <http://hla.stsci.edu/hlview.html>

gle component profile, the surface brightness profiles of the most massive and most extended models on a circular 60 kpc orbit, which have a comparable mass and effective radius as VUCD7, show a two-component profile. Figure 22 demonstrates that the surface brightness profile of model "CC_56_60-kpc" from Brüns et al. (2011) shows a very similar two-component structure as the observed VUCD7. Consequently, a two-component "core-halo" surface brightness profile cannot be used as evidence for the stripping scenario as also the merged cluster scenario explains this specific structure of the most extreme UCDs.

In addition, Brüns et al. (2009) discussed the origin of the EOs, or faint fuzzies, associated with the disk of NGC1023 in the context of merged cluster scenario and demonstrated that the observed structural parameters of the faint fuzzies are in excellent agreement with the modelled merger objects.

In conclusion, the merged star cluster origin for EOs explains the existence of EOs over the entire observed range of luminosities of ECs and UCDs, the trends in the structural parameters, and the differences between early and late-type galaxies at the high-luminosity end.

5. Summary & Conclusions

We searched the available literature to compile the largest possible catalog of star clusters with effective radii larger than 10 pc. As there is no clear distinction between ECs and UCDs, both types of objects are called extended stellar objects – abbreviated "EOs" – in this paper.

In total, we compiled a catalog of 813 EOs of which 171 were found associated with late-type galaxies and 642 EOs associated with early-type galaxies. The main results presented in this paper are

1. EOs cover a luminosity range from about $M_V = -4$ to -14 mag. However, almost all EOs brighter than $M_V = -10$ mag are associated with giant elliptical galaxies.
2. At all values of M_V extended objects are found with effective radii between 10 pc and an upper size limit, which shows a clear trend: the more luminous the object the larger is the upper size limit. This upper limit increases from about 30 pc at $M_V = -5$ mag to about 100 pc at $M_V = -14$ mag.
3. The 175 confirmed EOs cover the same region in the r_{eff} vs. M_V space and show the same trends of increasing size with increasing luminosities as the 638 candidate EOs.
4. For all luminosities, the majority of EOs have effective radii which are only slightly larger than 10 pc. The median effective radius of EOs in late-type and early-type galaxies is 13.2 pc and 14.2 pc, respectively.
5. The effective radii are increasing with increasing total luminosity of the host galaxy.
6. For late-type galaxies there is no trend of the EO luminosities with the luminosity of the host galaxies, while for early-type galaxies there is a trend that the most luminous EOs are found associated with the most luminous galaxies.
7. EOs and GCs form a coherent structure in the r_{eff} vs. M_V parameter space, which is well separated from the distribution of early type dwarf galaxies, except for the rare species of compact elliptical galaxies. Especially at the low-luminosity end considerably deeper observations are needed to answer the question, whether the prominent gap between ECs and dSph galaxies is real.
8. For both EOs associated with early and late-type galaxies, the EO luminosity functions peaks at about -6.5 mag, which is roughly one magnitude fainter than the turnover of the

GC luminosity function. The turnover luminosities decrease continuously between compact GCs and EOs for increasing effective radii. Considering the very low surface brightness of faint and extended EOs, a fair fraction of very extended and faint EOs is most likely below the detection limit of extra-galactic surveys. The true turnover of the EO luminosity function might therefore be at even lower luminosities.

We discussed an EO formation scenario on the basis of a star cluster origin which explains the existence of EOs, the trends of the structural parameters and the differences between early and late-type galaxies over the entire range of luminosities of ECs and UCDs. In addition, a core-halo surface brightness profile, as observed for some massive EOs like VUCD7, can be reproduced in the merged CC formation scenario.

While this study presents the to day largest catalog of EOs, it suffers from substantial incompleteness, predominantly with respect to the coverage of the galactic halos, but also with respect to varying detection limits and the fairly low number of confirmed objects. Larger and more complete data-sets and additional information on parameters like metallicities, mass-to-light ratios and age-estimates are necessary to draw final conclusions on the origin of EOs, which in turn has the potential to shed light on the cosmologically important phase of galaxy formation.

Acknowledgements. This work was supported by the German *Deutsche Forschungsgemeinschaft*, DFG project number KR 1635/29-1. We thank J.P. Madrid and S. Larsen for providing additional data on EOs not directly accessible from Madrid (2011) and Larsen & Brodie (2000). We thank the anonymous referee for his helpful comments, which lead to a considerably improved paper.

References

- Bastian, N., Emsellem, E., Kissler-Patig, M., & Maraston, C. 2006a, A&A, 445, 471
- Bastian, N., Saglia, R. P., Goudfrooij, P., Kissler-Patig, M., Maraston, C., Schweizer, F., & Zoccali, M. 2006b, A&A, 448, 881
- Bastian, N., Tranco, G., Konstantopoulos, I.S., & Miller, B.W. 2009, ApJ, 701, 607
- Bekki, K., Couch, W. J., & Drinkwater, M. J. 2001, ApJ, 552, L105
- Bekki, K., Couch, W. J., Drinkwater, M. J., & Shioya, Y. 2003, MNRAS, 344, 399
- Bekki, K., Couch, W. J., Drinkwater, M. J., & Shioya, Y. 2004, ApJ, 610, L13
- Bell, E. F., Slater, C. T., Martin, N. F. 2011, ApJ, 742, L15
- Belokurov, V., Walker, M. G., Evans, N. W. et al. 2010, ApJ, 712, L103
- Blakeslee, J. P., & Barber DeGraaff, R. 2008, AJ, 136, 2295
- Blom C., Spitler, L. R., & Forbes, D. A. 2012, MNRAS, 420, 37
- Bournaud, F., Bois, M., Emsellem, E., & Duc, P.-A. 2008a, Astron. Nachr., 329, 1025
- Bournaud, F., Duc, P.-A., & Emsellem, E. 2008b, MNRAS, 389, L8
- Brasseur, C. M., Martin, N. F., Macciò, A. V., Rix, H.-W., Kang, X. 2011, ApJ, 743,179
- Brodie, J. P., & Larsen, S. S. 2002, AJ, 124, 1410
- Brodie, J. P., & Strader, J. 2006, ARA&A, 44, 193
- Brodie, J. P., Romanowsky, A. J., Strader, J., & Forbes, D. A. 2011, AJ, 142, 199
- Brüns, R. C., Kroupa, P., & Fellhauer, M. 2009, ApJ, 702, 1268
- Brüns, R. C., & Kroupa, P. 2011, ApJ, 729, 69
- Brüns, R. C., Kroupa, P., Fellhauer, M., Metz, M., & Assmann, P. 2011, A&A, 529, 138
- Cantiello, M., Brocato, E., & Blakeslee, J. P. 2009, A&A, 503, 87
- Cappellari, M., Bacon, R., Bureau, M. et al. 2006, MNRAS, 366, 1126
- Chandar, R., Whitmore, B., & Lee, M. G. 2004, ApJ, 611, 220
- Chattopadhyay, A.K., Chattopadhyay, T., Davoust, E., Mondal, S., Sharina, M. 2009, ApJ, 705, 1533
- Chiboucas, K., Tully, R. B., Marzke, R. O. et al. 2011, ApJ, 737, 86
- Chies-Santos, A. L., Pastoriza, M. G., Santiago, B. X., & Forbes, D. A. 2006, A&A, 455, 453
- Chies-Santos, A. L., Santiago, B. X., & Pastoriza, M. G. 2007, A&A, 467, 1003
- Chies-Santos, A. L., Larsen, S. S., Wehner, E. M. et al. 2011, A&A, 525, 19
- Chilingarian, I. V., & Mamon, G. A. 2008, MNRAS, 385, L83
- Chilingarian, I. V., Mieske, S., Hilker, M., & Infante, L. 2011, MNRAS, 412, 1627

- Cockcroft, R., Harris, W. E., Ferguson, A. M. N., et al. 2011, *ApJ*, 730, 112
- Dabringhausen, J., Hilker, M., & Kroupa, P. 2008, *MNRAS*, 386, 864
- Dabringhausen, J., Kroupa, P., & Baumgardt, H. 2009 *MNRAS*, 394, 1529
- Da Costa, G. S., Grebel, E. K., Jerjen, H., Rejkuba, M., & Sharina, M. E. 2009, *AJ*, 137, 4361
- Da Rocha, C., Mieske, S., Georgiev, I. Y. et al. 2011, *A&A*, 525, 86
- DeGraaff, R.B., Blakeslee, J.P., Meurer, G.R., & Putman, M.E., 2007, *ApJ*, 671, 1624
- de Grijs, R., Anders, P., Bastian, N., et al. 2003, *MNRAS*, 343, 1285
- Drinkwater, M. J., Jones, J. B., Gregg, M. D., & Phillipps, S. 2000, *PASA*, 17, 227
- Elmegreen, D. M. 2007, in *IAU symp. 235*, eds. F. Combes, & J. Palous, 376
- Evtstigneeva, E. A., Gregg, M. D., Drinkwater, M. J., & Hilker, M. 2007, *AJ*, 133, 1722
- Evtstigneeva, E. A., Drinkwater, M. J., Peng, C.Y., et al. 2008, *AJ*, 136, 461
- Fellhauer, M., & Kroupa, P. 2002a, *MNRAS*, 330, 642
- Fellhauer, M., & Kroupa, P. 2002b, *AJ*, 124, 2006
- Fellhauer, M., & Kroupa, P. 2005, *MNRAS*, 359, 223
- Forbes, D. A., Lasky, P., Graham, A. W., & Spitler, L. 2008, *MNRAS*, 389, 1924
- Geha, M., van der Marel, R. P., Guhathakurta, P., et al. 2010, *ApJ*, 711, 361
- Georgiev, I. Y., Puzia, T. H., Hilker, M., & Goudfrooij, P. 2009, *MNRAS*, 392, 879
- Gilmore, G., Wilkinson, M. I., Wyse, R. F. G., et al. 2007, *ApJ*, 663, 948
- Goudfrooij, P. 2012, *ApJ*, 750, 140
- Gómez, M., Geisler, D., Harris, W. E., et al. 2006, *A&A*, 447, 877
- Harris, W. E. 1996, *AJ*, 112, 1487
- Harris, W. E., Mouhcine, M., Rejkuba, M., & Ibata, R. 2009, *MNRAS*, 395, 436
- Haşegan, M., Jordán, A., Côté, P., et al. 2005, *ApJ*, 627, 203
- Hau, G. K. T., Spitler, L. R., Forbes, D. A., et al. 2009, *MNRAS*, 394, L97
- Hilker, M., Infante, L., Vieira, G., Kissler-Patig, M., & Richtler, T. 1999, *A&AS*, 134, 75
- Hilker, M., Baumgardt, H., Infante, L., et al. 2007, *A&A*, 463, 119
- Hurley, J.R., & Mackey, A.D. 2010, *MNRAS*, 408, 2353
- Huxor, A. P., Ferguson, A. M. N., Barker, M. K., et al. 2009, *ApJ*, 698, L77
- Huxor, A. P., Ferguson, A. M. N., Tanvir, N. R., et al. 2011a, *MNRAS*, 414, 770
- Huxor, A. P., Tanvir, N. R., Irwin, M. J., et al. 2005, *MNRAS*, 360, 1007
- Huxor, A. P., Tanvir, N. R., Ferguson, A. M. N., et al. 2008, *MNRAS*, 385, 1989
- Huxor, A. P., Phillipps, S., Price, J., & Harniman, R. 2011b, *MNRAS*, 414, 3557
- Hwang, N., & Lee, M. G. 2008, *AJ*, 135, 1567
- Hwang, N., Lee, M.G., Lee, J.C., et al. 2011, *ApJ*, 738, 58
- Jordán, A., Côté, P., Blakeslee, J. P., et al. 2005, *ApJ*, 634, 1002
- Kroupa, P. 1998, *MNRAS*, 300, 200
- Larsen, S. S., & Brodie, J. P. 2000, *AJ*, 120, 2938
- Larsen, S. S., Forbes, D. A., & Brodie, J. P. 2001, *MNRAS*, 327, 1116
- Mackey, A. D., & Gilmore, G. F. 2004, *MNRAS*, 352, 153
- Madrid, J. P., Graham, A. W., Harris, W. E., et al. 2010, *ApJ*, 722, 1707
- Madrid, J. P. 2011, *ApJ*, 737, L13
- Maraston, C., Bastian, N., Saglia, R. P., et al. 2004, *A&A*, 416, 467
- Martin, N. F., de Jong, J. T. A., & Rix, H.-W. 2008, *ApJ*, 684, 1075
- Masters, K. L., Jordán, A., Côté, P., et al. 2010, *ApJ*, 715, 1419
- McConnachie, A. W. 2012, *AJ*, 144, 4
- McConnachie, A. W., & Irwin, M. J. 2006, *MNRAS*, 365, 1263
- McLaughlin, D. E., & van der Marel, R. P. 2005, *ApJS*, 161, 304
- McLaughlin, D. E., Barmby, P., Harris, W. E., Forbes, D. A., & Harris, G. L. H. 2008, *MNRAS*, 384, 563
- Mengel, S., Lehnert, M. D., Thatte, N. A., et al. 2008, *A&A*, 489, 1091
- Mieske, S., Hilker, M., & Infante, L. 2002, *A&A*, 383, 823
- Mieske, S., Hilker, M., Jordán, A., Infante, L., & Kissler-Patig, M. 2007, *A&A*, 472, 111
- Mieske, S., Hilker, M., Jordán, A., et al. 2008, *A&A*, 487, 921
- Mieske, S., Hilker, M., Misgeld, I. 2012, *A&A*, 537, 3
- Mieske, S., Infante, L., Hilker, M., et al. 2005, *A&A*, 430, L25
- Mieske, S., & Kroupa, P. 2008, *ApJ*, 677, 276
- Misgeld, I., & Hilker, M. 2011, *MNRAS*, 414, 3699
- Misgeld, I., Mieske, S., Hilker, M. et al. 2011, *A&A*, 531, 4
- Mouhcine, M., Harris, W.E., Ibata, R. & Rejkuba, M. 2010, *MNRAS*, 404, 1157
- Murray, M. 2009, *ApJ*, 691, 946
- Nantais, J. B., Huchra, J.P., Zezas, A., Gazeas, K., & Strader, J. 2011, *AJ*, 142, 183
- Norris, M. A., & Kannappan, S. J. 2011, *MNRAS*, 414, 739
- Peacock, M.B., Maccarone, T.J., Waters, C.Z., Kundu, A., Zepf, S.E., Knigge, C., & Zurek, D.R. 2009, *MNRAS*, 392, 55
- Pellerin, A., Meurer, G. R., Bekki, K., et al. 2010, *AJ*, 139, 1369
- Peng, E. W., Côté, P., Jordán, A., et al. 2006, *ApJ*, 639, 838
- Penny, S. J., Forbes, D. A., & Conselice, C. J. 2012, *MNRAS*, 422, 885
- Phillipps, S., Drinkwater, M. J., Gregg, M. D., & Jones, J. B. 2001, *ApJ*, 560, 201
- Portegies Zwart, S. F., McMillan, S. L. W., & Gieles, M. 2010, *ARA&A*, 48, 431
- Price, J., Phillipps, S., Huxor, A. et al. 2009, *MNRAS*, 397, 1816
- Rejkuba, M. 2012, *Ap&SS*, astro-ph/1201.3936
- Richtler, T., Dirsch, B., Larsen, S., Hilker, M., & Infante, L. 2005, *A&A*, 439, 533
- Salinas, R., Jilkova, L., Carraro, G., Catelan, M., Amigo, P. 2012. *MNRAS*, 421, 960
- Secker, J. 1992, *AJ*, 104, 1472
- Sharina, M. E., Puzia, T. H., & Makarov, D. I. 2005, *A&A*, 442, 85
- Sharina, M. E., Karachentsev, I. D., Dolphin, A. E. et al. 2008, *MNRAS*, 384, 1544
- Slater, C. T., Bell, E. F., Martin, N. F. 2011, *ApJ*, 742, L14
- Smith Castelli, A. V., Faifer, F. R., Richtler, T., & Bassino, L. P. 2008, *MNRAS*, 391, 685
- Smith Castelli, A. V., Cellone, S. A., Faifer, F. R. et al. 2012, *MNRAS*, 419, 2472
- Stonkutė, R., Vanevičius, V., Arimoto, N., et al. 2008, *AJ*, 135, 1482
- Strader, J., Seth, A. C., Caldwell, N. 2012, *AJ*, 143, 52
- Taylor, M. A., Puzia, T. H., Harris, G. L., et al. 2010, *ApJ*, 712, 1191
- Tran, H. D., Sirianni, M., Ford, H. C. et al. 2003, *ApJ*, 585, 750
- van den Bergh, S. 2006, *AJ*, 131, 304
- van den Bergh, S., & Mackey, A. D. 2004, *MNRAS*, 354, 713
- Whitmore, B. C. 2003, in *A Decade of Hubble Space Telescope Science*, ed. M. Livio, K. Noll, & M. Stiavelli, 153
- Whitmore, B. C., Gilmore, D., Leitherer, C., et al. 2005, *AJ*, 130, 2104
- Whitmore, B. C., Chandar, R., Schweizer, F., et al. 2010, *AJ*, 140, 75
- Wilson, C. D., Scoville, N., Madden, S. C., & Charmandaris, V. 2003, *ApJ*, 599, 1049
- Wilson, C. D., Harris, W. E., Longden, R., & Scoville, N. Z. 2006, *ApJ*, 641, 763